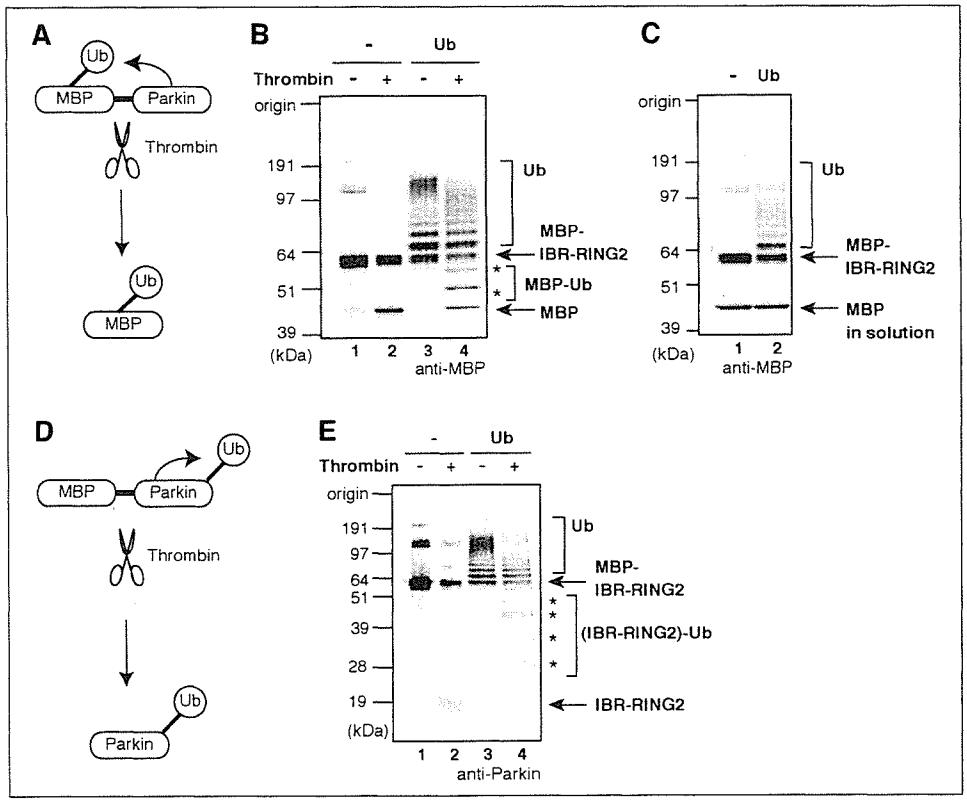

FIGURE 2. **In-frame-fused MBP can be a good pseudosubstrate of Parkin.** *A*, a schematic diagram of Parkin catalyzed ubiquitylation of MBP. If the MBP portion is ubiquitylated, a change in its mobility would be recognized by immunoblotting after cleavage. *B*, the MBP-(IBR-RING2) fused protein (see Fig. 4) was subjected to *in vitro* ubiquitylation, subsequent cleavage into MBP moiety, and immunoblotting with anti-MBP antibody. The MBP portion of IBR-RING2 was ubiquitylated (*asterisks*). *C*, MBP can be ubiquitylated only when it is in the physical vicinity of Parkin. Note that free MBP in solution was not ubiquitylated. *D*, a schematic diagram of Parkin-catalyzed autoubiquitylation. *E*, IBR-RING2 portion is also ubiquitylated. *Asterisks* in *lane 4* show the ubiquitylated IBR-RING2 moiety (compare *lane 4* with *2*). Ubc7 was used as E2 in these experiments.

activity than GST-Parkin, as shown in Fig. 1*F*, we used MBP-Parkin in the following experiments.

Fused MBP Is a Good Pseudo-substrate to Monitor E3 Activity of Parkin—We next determined whether the MBP portion or Parkin portion (or both) is ubiquitylated. To check this, we purified MBP-LVPRGS-Parkin, in which a thrombin-digestion sequence is inserted between MBP and Parkin. As depicted in Fig. 2*A*, if the MBP moiety is ubiquitylated, its molecular weight would increase by ubiquitylation and subsequent digestion, but if not ubiquitylated, its molecular weight would remain unchanged. First we tried to split MBP-LVPRGS-Parkin by thrombin; however, this recombinant protein was hardly digested for some unknown reason (data not shown). We next fused the C-terminal IBR-RING2 region of Parkin to MBP-LVPRGS (hereafter dubbed IBR-RING2, see Fig. 4*A*), and this construct was cleaved moderately (Fig. 2*B*, *lanes 1* and *2*). When IBR-RING2 was subjected to an ubiquitylation assay and subsequently separated into MBP and IBR-RING2 portions by thrombin digestion, the molecular weight of MBP moiety was clearly increased (see the *asterisks* in Fig. 2*B*, *lanes 3* and *4*), meaning that the MBP portion is ubiquitylated. Does this result mean that bacterial MBP protein is the substrate for Parkin? The answer is no. When sole MBP protein was incubated with IBR-RING2, this free MBP was not ubiquitylated at all, even though IBR-RING2 was autoubiquitylated as described (Fig. 2, compare *C* with *B*). This result indicates that the IBR-RING2 region of Parkin ubiquitylates fused-MBP, but not unbound MBP, and strongly suggests that Parkin recognizes MBP as a substrate not because of its amino acid sequence but because of its physical vicinity to Parkin. As depicted in Fig. 2*D*, when the same experiment was repeated using an anti-Parkin antibody, the molecular weight of the IBR-RING2 moiety was also increased meaning that both MBP and IBR-RING2 portions were ubiquitylated (Fig. 2*E*). Although many putative substrates of Parkin have been reported, the lack of a good *in vitro* substrate makes any biochemical study difficult. Our study revealed that fused MBP could be a good pseudo-substrate to monitor the E3 activity of Parkin.

Parkin by Itself Catalyzes Multiple Monoubiquitylation—The Uev1-Ubc13 heterodimer is an E2 involved in the formation of Lys-63-linked polyubiquitylation (19). We confirmed that our Uev1-Ubc13 complex is functional (Fig. 1*D* and supplemental Fig. 1*A*). Motivated by the findings that Parkin catalyzes Lys-63-linked polyubiquitylation (20, 21) and Parkin cooperates with Uev1-Ubc13 in our assay (Fig. 1*B*), we investigated the mode of Parkin-catalyzed ubiquitylation. Parkin could either catalyze multiple monoubiquitylation, Lys-48-linked polyubiquitylation, or Lys-63-linked polyubiquitylation. Lys-48-linked polyubiquitylation has been studied most and it essentially directs the substrate to degradation by the proteasome. In contrast, the Lys-63-linked polyubiquitylation and monoubiquitylation serve as a signal other than proteasomal-proteolysis (22–24). We first used methylated ubiquitin (hereafter referred to as Met-Ub) in which all lysine residues are blocked by methylation and is incapable of polyubiquitylation. If Parkin catalyzes polyubiquitylation, the use of Met-Ub would shorten the ladder of ubiquitylation but if not, the ubiquitylation pattern would remain unchanged. Unexpectedly, the use of Met-Ub and Uev1-Ubc13 did not change the ubiquitylation pattern, indicating that Parkin catalyzes multiple monoubiquitylation *in vitro* (Fig. 3*A*). The same result was observed when Ubc7 was used as E2 (Fig. 3*B*), and these results were more evident when IBR-RING2 (Fig. 4*A*) was utilized (Fig. 3, *C* and *D*). Repeated experiments using lysine-less ubiquitin, in which all lysine residues were changed to arginine, showed it cannot form a polyubiquitin chain, again confirmed the consequence (Fig. 3*E*). It is noteworthy that sole Ubc13 itself assisted autoubiquitylation of Parkin as well as the Uev1-Ubc13 complex (supplemental Fig. 1*B*), again supporting this conclusion. These results allowed us to conclude that the mode of ubiquitylation catalyzed by intrinsic Parkin *in vitro* is multiple monoubiquitylation rather than polyubiquitylation (see "Discussion").

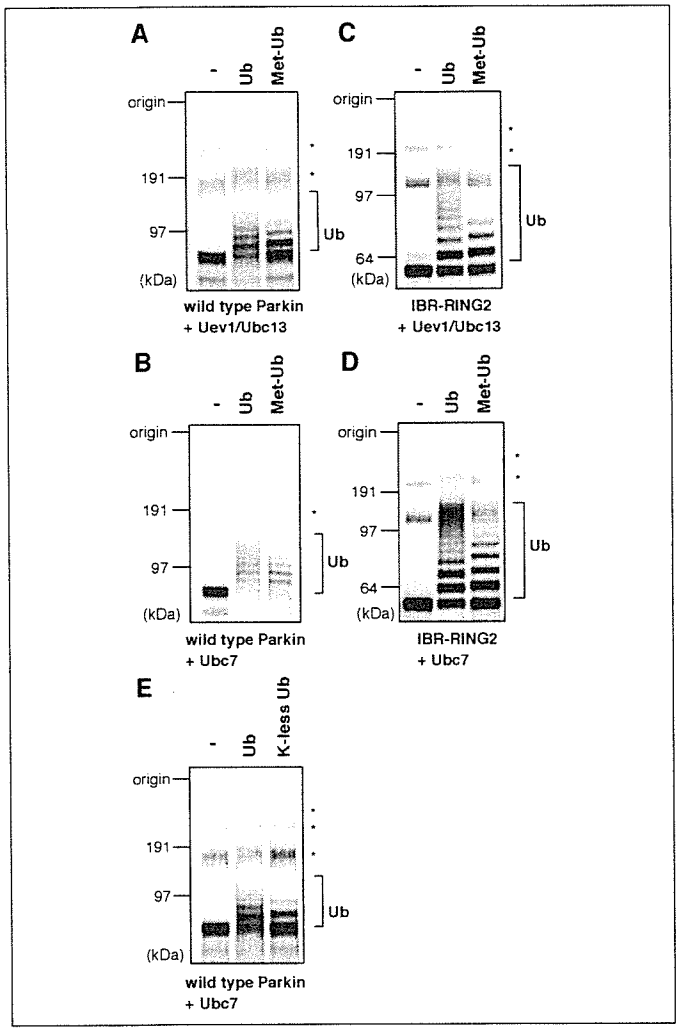

FIGURE 3. **Parkin catalyzes multiple monoubiquitylation.** *A* and *B*, *in vitro* ubiquitylation assay was performed in the absence (−) or presence of ubiquitin (*Ub*) or methylated-ubiquitin (*Met-Ub*; cannot form polyubiquitylation chain). Uev1-Ubc13 was used as E2 in *A* and Ubc7 in *B*. Almost identical ubiquitylation patterns were observed in Ub and Met-Ub, indicating that Parkin catalyzes multiple monoubiquitylation. *C* and *D*, the result was more evident when IBR-RING2 (see Fig. 4) was utilized. Uev1-Ubc13 was used as E2 in *C* and Ubc7 in *D*. *E*, the same experiment was performed using lysine-less ubiquitin. *Ub*, autoubiquitylation; *, oligomerization bands. Anti-MBP antibody was used in all experiments.

Mode of E3 Activity of Parkin with Pathogenic Missense Mutations—At present, dozens of disease-relevant mutations of Parkin have been reported, and the primary cause of autosomal recessive juvenile parkinsonism is assumed to be impairment of the E3 activity of Parkin by such mutations. However, it is still contentious whether Parkin with PD-causing mutation loses its E3 activity or not (see supplemental Table 1), primarily because of the absence of a sensitive E3-activity assay system using recombinant Parkin. To settle this problem, we examined the E3 activity of MBP-Parkin harboring various mutations and deletions. Three in-frame exonic deletions and 19 PD-linked mutations distributed throughout Parkin were selected (Fig. 4*A*). In addition, two Parkin species, one lacks its Ubl domain (ΔUbl) and the other possesses only C-terminally IBR-RING2 domain (IBR-RING2), were also generated. When these MBP-Parkin mutants were incubated with Ubc7 as E2, only mutations neighboring the second RING finger motif (Fig. 4*A*, *solid circles*) abolished the E3 activity completely (Fig. 4*B*). A nonsense mutation lacking the rear RING finger motif had no E3 activity and sole IBR-RING2 retained the E3 activity (Fig. 4, *light gray circles*), indicating that the second RING finger motif is the catalytic core for the E3 activity of Parkin. Contrary to what was assumed, all disease-relevant mutations other than those in RING2 still possessed E3 activities equivalent to that of the wild-type Parkin (Fig. 4*B*). The same results were observed when UbcH7 or Uev1-Ubc13 was used as E2 (data not shown). In these assays, we used a bacterially expressed recombinant Parkin, and to our knowledge, this is the first direct evidence that E3 activity of the strictly pure Parkin harboring various pathogenic mutations is not compromised.

DISCUSSION

To date, numerous biochemical studies have been performed to understand the E3 activity of Parkin. However, it is difficult to rule out the possible involvement of other E3s (see Introduction). Furthermore, the lack of a good model substrate spurs the difficulty to check the intrinsic E3 activity of Parkin. We thus set up a sensitive E3 assay system using bacterially expressed recombinant Parkin. Our assay system has some advantages; namely, we can obtain a large quantity of MBP-Parkin with higher E3 activity than GST-Parkin (Fig. 1). In addition, this fusion protein was already primed for ubiquitylation even in the absence of model substrate, because fused MBP can work as a good pseudo-substrate (Fig. 2). More importantly, because MBP-Parkin is purified from *E. coli*, it is free from possible contamination of other E3(s). The establishment of this assay allowed us to perform a thorough biochemical characterization of Parkin protein.

Interestingly, sole Parkin catalyzes multiple monoubiquitylation *in vitro* (Fig. 3). Moreover, although Doss-Pepe *et al.* (20) reported that Parkin accelerates polyubiquitin chain formation, the MBP-Parkin in our assay did not stimulate the assembly of polyubiquitin chain (Fig. 1*D*, compare *lanes 4* and *6*, and *10* and *12*, respectively). These results seemingly suggest that the ubiquitylation catalyzed by Parkin functions not for proteasomal degradation but for non-proteasomal-proteolytic function(s), such as transcriptional regulation and/or membrane trafficking *in vivo*. However, it is still premature to make such conclusion. Although we showed that pure Parkin catalyzes multiple monoubiquitylation *in vitro* (Fig. 3), some additional factor(s) like E4 can work together *in vivo*, and this needs to be considered. E4 can extend the ubiquitin chain by recognizing the ubiquitin moiety of a ubiquitylated-protein as a substrate (25). If such an E4-like factor(s) cooperates with Parkin *in vivo*, it is still possible that monoubiquitylation catalyzed by Parkin is used as the scaffold for further polyubiquitylation and finally functions for proteasomal degradation. All things considered, further studies are obviously required; in particular, the authentic substrate and the function of Parkin-catalyzed ubiquitylation need to be addressed.

Another unexpected result was that most of the PD-relevant missense mutations do not abrogate E3 activity of Parkin (Fig. 4). Only missense mutations in the rear RING finger motif abolished the E3 activity, revealing that not the first but the second RING finger motif is the catalytic core of Parkin. Recently, several studies that focused on the pathophysiological mechanisms of Parkin have been published (26–30). Although our results on enzymatic activities of mutant Parkin are not fully consistent with previous reports (see supplemental Table 1), methodological differences in the E3 assay may account for the conflicting observation. For example, in one study immunoprecipitated Parkin was used as the source of E3 *in vitro* (31) and in other studies, E3 activity of Parkin was checked by whether or not coexpression of Parkin in cells enhances the ubiquitylation of the putative substrate (7, 30). Although there is little discrepancy, recent studies and our present work drew the same conclusion that the dysfunction of Parkin is not simply attributable to catalytic impairment of its E3 activity. Indeed, several missense mutations cause Parkin to be sequestered into an aggresome-like structure, and this phenomenon may be involved in disease pathogenesis

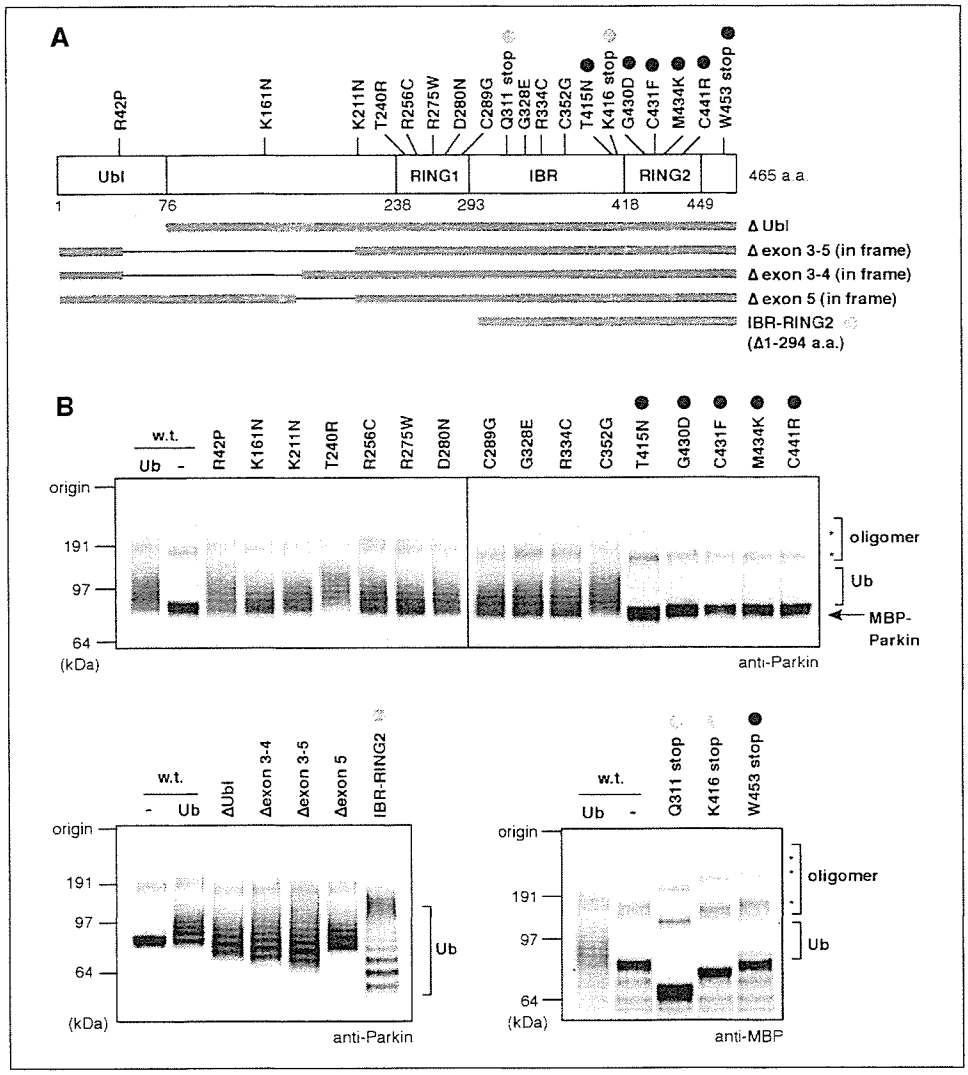

FIGURE 4. *A*, schematic diagram of disease-relevant mutations and exonic deletions of Parkin. *B*, E3 activities of various Parkin proteins bearing PD-linked mutations and deletions. Note that mutations neighboring the second RING finger motif (*solid circles*) abolished E3 activity of Parkin. *Light gray circles* indicate that the RING2 is the catalytic core of Parkin (see text for details). Conversely, pathogenic mutants other than RING2 mutants retain E3 activities equivalent to that of the wild-type (*w.t.*) control. *Ub*, autoubiquitylation; *, oligomerization bands.

(27–30). We think that disease-relevant mutations cause not only attenuation of E3 activity but also a variety of primary defects such as sequestration into aggresome and dissociation from its partner protein, and possibly a complex of such defects may eventually lead to Parkin dysfunction and autosomal recessive juvenile parkinsonism.

PD is the second most prevalent neurodegenerative disorder, and thus, analysis of Parkin is important in terms of public welfare. Indeed, a large number of articles on Parkin have been published; however, because of fierce scientific competition, not all Parkin-related phenomena were critically scrutinized although there remains room for close examination. For example, Pawlyk *et al.* (32) recently inspected the anti-Parkin antibodies and uncovered a high non-specificity of the available Parkin antibodies. This also holds true for the E3 activity of Parkin, because precedent works could not exclude the possible involvement of another E3(s). Herein we investigated thoroughly the enzymatic activity of bacterially expressed recombinant Parkin. Although our work is not conspicuous, we hope that our biochemical characterization using pure Parkin would be a solid cornerstone for further studies, as the preceding works were.

Acknowledgments—We thank Dr. Tsunehiro Mizushima of Nagoya University for providing recombinant Ubc7 protein. We also thank all members of Prof. K. Tanaka laboratory for the helpful discussions.

REFERENCES

1. Moore, D. J., West, A. B., Dawson, V. L., and Dawson, T. M. (2005) *Annu. Rev. Neurosci.* **28,** 57–87
2. Giasson, B. I., and Lee, V. M. (2003) *Cell* **114,** 1–8
3. Ross, C. A., and Pickart, C. M. (2004) *Trends Cell Biol.* **14,** 703–711
4. Tanaka, K., Suzuki, T., Hattori, N., and Mizuno, Y. (2004) *Biochim. Biophys. Acta* **1695,** 235–247
5. Hattori, N., and Mizuno, Y. (2004) *Lancet* **364,** 722–724
6. Lohmann, E., Periquet, M., Bonifati, V., Wood, N. W., De Michele, G., Bonnet, A. M., Fraix, V., Broussolle, E., Horstink, M. W., Vidailhet, M., Verpillat, P., Gasser, T., Nicholl, D., Teive, H., Raskin, S., Rascol, O., Destee, A., Ruberg, M., Gasparini, F., Meco, G., Agid, Y., Durr, A., and Brice, A. (2003) *Ann. Neurol.* **54,** 176–185
7. Ren, Y., Zhao, J., and Feng, J. (2003) *J. Neurosci.* **23,** 3316–3324
8. Corti, O., Hampe, C., Koutnikova, H., Darios, F., Jacquier, S., Prigent, A., Robinson, J. C., Pradier, L., Ruberg, M., Mirande, M., Hirsch, E., Rooney, T., Fournier, A., and Brice, A. (2003) *Hum. Mol. Genet.* **12,** 1427–1437
9. Imai, Y., Soda, M., Hatakeyama, S., Akagi, T., Hashikawa, T., Nakayama, K. I., and Takahashi, R. (2002) *Mol. Cell* **10,** 55–67
10. Zhong, L., Tan, Y., Zhou, A., Yu, Q., and Zhou, J. (2005) *J. Biol. Chem.* **280,** 9425–9430
11. You, J., Cohen, R. E., and Pickart, C. M. (1999) *BioTechniques* **27,** 950–954
12. Matsuda, N., Suzuki, T., Tanaka, K., and Nakano, A. (2001) *J. Cell Sci.* **114,** 1949–1957
13. Imai, N., Matsuda, N., Tanaka, K., Nakano, A., Matsumoto, S., and Kang, W. (2003) *J. Virol.* **77,** 923–930
14. Matsuda, N., Azuma, K., Saijo, M., Iemura, S., Hioki, Y., Natsume, T., Chiba, T., Tanaka, K., and Tanaka, K. (2005) *DNA Repair (Amst.)* **4,** 537–545
15. Shimura, H., Hattori, N., Kubo, S., Yoshikawa, M., Kitada, T., Matsumine, H., Asakawa, S., Minoshima, S., Yamamura, Y., Shimizu, N., and Mizuno, Y. (1999) *Ann.*

Neurol. **45,** 668–672
16. Rankin, C. A., Joazeiro, C. A., Floor, E., and Hunter, T. (2001) *J. Biomed. Sci.* **8,** 421–429
17. Araki, K., Kawamura, M., Suzuki, T., Matsuda, N., Kanbe, D., Ishii, K., Ichikawa, T., Kumanishi, T., Chiba, T., Tanaka, K., and Nawa, H. (2003) *J. Neurochem.* **86,** 749–762
18. Takai, R., Matsuda, N., Nakano, A., Hasegawa, K., Akimoto, C., Shibuya, N., and Minami, E. (2002) *Plant J.* **30,** 447–455
19. Hofmann, R. M., and Pickart, C. M. (1999) *Cell* **96,** 645–653
20. Doss-Pepe, E. W., Chen, L., and Madura, K. (2005) *J. Biol. Chem.* **280,** 16619–16624
21. Lim, K. L., Chew, K. C., Tan, J. M., Wang, C., Chung, K. K., Zhang, Y., Tanaka, Y., Smith, W., Engelender, S., Ross, C. A., Dawson, V. L., and Dawson, T. M. (2005) *J. Neurosci.* **25,** 2002–2009
22. Chen, Z. J. (2005) *Nat. Cell Biol.* **7,** 758–765
23. Hicke, L. (2001) *Nat. Rev. Mol. Cell Biol.* **2,** 195–201
24. Pickart, C. M. (2000) *Trends Biochem. Sci.* **25,** 544–548
25. Richly, H., Rape, M., Braun, S., Rumpf, S., Hoege, C., and Jentsch, S. (2005) *Cell* **120,** 73–84
26. Cookson, M. R., Lockhart, P. J., McLendon, C., O'Farrell, C., Schlossmacher, M., and Farrer, M. J. (2003) *Hum. Mol. Genet.* **12,** 2957–2965
27. Gu, W. J., Corti, O., Araujo, F., Hampe, C., Jacquier, S., Lucking, C. B., Abbas, N., Duyckaerts, C., Rooney, T., Pradier, L., Ruberg, M., and Brice, A. (2003) *Neurobiol. Dis.* **14,** 357–364
28. Henn, I. H., Gostner, J. M., Lackner, P., Tatzelt, J., and Winklhofer, K. F. (2005) *J. Neurochem.* **92,** 114–122
29. Wang, C., Tan, J. M., Ho, M. W., Zaiden, N., Wong, S. H., Chew, C. L., Eng, P. W., Lim, T. M., Dawson, T. M., and Lim, K. L. (2005) *J. Neurochem.* **93,** 422–431
30. Sriram, S. R., Li, X., Ko, H. S., Chung, K. K., Wong, E., Lim, K. L., Dawson, V. L., and Dawson, T. M. (2005) *Hum. Mol. Genet.* **14,** 2571–2586
31. Staropoli, J. F., McDermott, C., Martinat, C., Schulman, B., Demireva, E., and Abeliovich, A. (2003) *Neuron* **37,** 735–749
32. Pawlyk, A. C., Giasson, B. I., Sampathu, D. M., Perez, F. A., Lim, K. L., Dawson, V. L., Dawson, T. M., Palmiter, R. D., Trojanowski, J. Q., and Lee, V. M. (2003) *J. Biol. Chem.* **278,** 48120–48128

nature

Vol 441 15 June 2006 doi:10.1038/nature04723

LETTERS

Loss of autophagy in the central nervous system causes neurodegeneration in mice

Masaaki Komatsu[1,2]*, Satoshi Waguri[3]*†, Tomoki Chiba[1], Shigeo Murata[1], Jun-ichi Iwata[1,2], Isei Tanida[2], Takashi Ueno[2], Masato Koike[3], Yasuo Uchiyama[3], Eiki Kominami[2] & Keiji Tanaka[1]

Protein quality-control, especially the removal of proteins with aberrant structures, has an important role in maintaining the homeostasis of non-dividing neural cells[1]. In addition to the ubiquitin–proteasome system, emerging evidence points to the importance of autophagy—the bulk protein degradation pathway involved in starvation-induced and constitutive protein turnover—in the protein quality-control process[2,3]. However, little is known about the precise roles of autophagy in neurons. Here we report that loss of *Atg7* (autophagy-related 7), a gene essential for autophagy, leads to neurodegeneration. We found that mice lacking *Atg7* specifically in the central nervous system showed behavioural defects, including abnormal limb-clasping reflexes and a reduction in coordinated movement, and died within 28 weeks of birth. *Atg7* deficiency caused massive neuronal loss in the cerebral and cerebellar cortices. Notably, polyubiquitinated proteins accumulated in autophagy-deficient neurons as inclusion bodies, which increased in size and number with ageing. There was, however, no obvious alteration in proteasome function. Our results indicate that autophagy is essential for the survival of neural cells, and that impairment of autophagy is implicated in the pathogenesis of neurodegenerative disorders involving ubiquitin-containing inclusion bodies.

Macroautophagy (hereafter referred to as autophagy) is an evolutionarily conserved pathway in which the cytoplasm and organelles are engulfed within double-membraned vesicles, known as autophagosomes, in preparation for the turnover and recycling of these cellular constituents[4]. Genetic studies using various model organisms have highlighted the importance of autophagy in physiological and pathological events[5]. The principal role of autophagy is in the supply of nutrients for survival, as shown in yeast[6] and early neonatal mice[7,8]. Autophagy also has a role in cellular remodelling during differentiation and the development of multicellular organisms, such as dauer formation in *Caenorhabditis elegans*[9] and metamorphosis in *Drosophila melanogaster*[10]. Moreover, constitutive autophagy, which occurs independently of nutrient stress, contributes to mouse liver homeostasis[8], major histocompatibility class (MHC) II antigen presentation[11], and cellular defence against invading streptococci[12] and *Mycobacterium tuberculosis*[13]. However, the physiological functions of autophagy, particularly in neurons, are still largely unknown.

To examine the relationship between neuronal pathology and autophagy deficiency *in vivo*, we crossed *Atg7*-conditional knockout mice ($Atg7^{flox/flox}$) (ref. 8) with transgenic mice expressing Cre recombinase under the control of the nestin promoter (nestin-*Cre*) (ref. 14), to produce mice deficient for *Atg7* specifically in the central nervous system ($Atg7^{flox/flox}$; nestin-*Cre*). Atg7 is an E1-like enzyme for both the Atg12- and Atg8-conjugation systems[15], and is essential

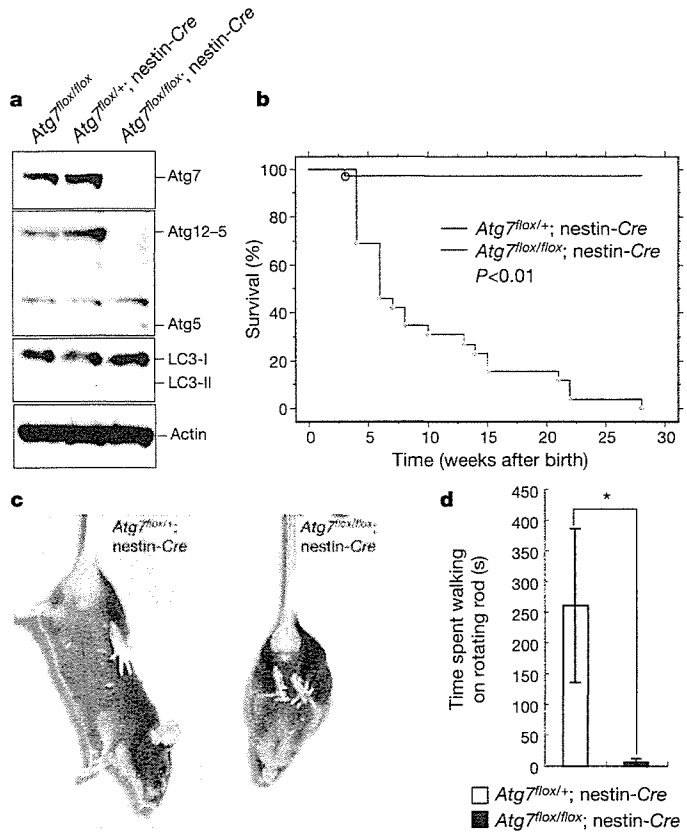

Figure 1 | Behavioural disorder in $Atg7^{flox/flox}$; nestin-*Cre* mice. **a**, Impairment of two ATG-conjugation systems (Atg12 and LC3) in the Atg7-deficient brain. Brain homogenates from P28 mice were immunoblotted with antibodies against Atg7, Atg5 and LC3. Actin was used as a loading control. Data shown are representative of three separate experiments. **b**, Kaplan–Meier survival curves of $Atg7^{flox/+}$; nestin-*Cre* ($n = 41$) and $Atg7^{flox/flox}$; nestin-*Cre* ($n = 26$) mice over 28 weeks. **c**, Abnormal limb-clasping reflexes in $Atg7^{flox/flox}$; nestin-*Cre* mice at P28. When lifted by the tail, $Atg7^{flox/+}$; nestin-*Cre* mice behave normally, extending their hind limbs and bodies. In contrast, $Atg7^{flox/flox}$; nestin-*Cre* mice bend their legs towards their trunk or tighten their back limbs to their bodies and anterior limbs. **d**, Movement ataxia in $Atg7^{flox/flox}$; nestin-*Cre* mice at P28. Motor coordination was tested using a rotarod assay. $Atg7^{flox/+}$; nestin-*Cre* ($n = 5$) and $Atg7^{flox/flox}$; nestin-*Cre* ($n = 5$) mice were placed on a rod rotating at 20 r.p.m., and the time spent on the rod was counted. Data show mean ± s.d. *, $P < 0.01$ (Student's *t*-test). There was no significant sex difference in survival rate and onset-stage of abnormal limb-clasping and tremor in $Atg7^{flox/flox}$; nestin-*Cre* mice.

[1]Laboratory of Frontier Science, Tokyo Metropolitan Institute of Medical Science, Bunkyo-ku, Tokyo 113-8613, Japan. [2]Department of Biochemistry, Juntendo University School of Medicine, Bunkyo-ku, Tokyo 113-8421, Japan. [3]Department of Cell Biology and Neurosciences, Osaka University Graduate School of Medicine, Osaka 565-0871, Japan. †Present address: Department of Anatomy and Histology, Fukushima Medical University School of Medicine, 1 Hikarigaoka, Fukushima 960-1295, Japan.
*These authors contributed equally to this work.

for autophagy[8]. Atg7 protein was absent at postnatal day (P)28 in brain from *Atg7*$^{flox/flox}$; nestin-*Cre* but not control (*Atg7*$^{flox/+}$; nestin-*Cre*) mice (Fig. 1a). The level of Atg7 protein in other tissues such as liver, lung, heart and muscle was comparable between *Atg7*$^{flox/flox}$; nestin-*Cre* and control mice (data not shown). Atg12–Atg5 conjugate was detected only in the brains of control mice by immunoblotting with an anti-Atg5 antibody (Fig. 1a). In contrast, free Atg5, which was faintly observed in the control mouse brain, was clearly increased in the mutant brain (Fig. 1a). The mammalian homologue of yeast Atg8, microtubule-associated protein 1 light-chain 3 (LC3), exists in two forms (LC3-I and LC3-II)[16]. Both forms were detected in brains from control mice, but only the LC3-I form was detected in *Atg7*$^{flox/flox}$; nestin-*Cre* brain (Fig. 1a). The loss of both Atg7 and LC3-II proteins was observed from P0 in the brain of *Atg7*$^{flox/flox}$; nestin-*Cre* mice (Supplementary Fig. S1). These results indicate complete impairment of autophagy in the central nervous system of *Atg7*$^{flox/flox}$; nestin-*Cre* mice after birth.

Atg7$^{flox/flox}$; nestin-*Cre* mice were viable at birth and indistinguishable in appearance from their littermates. However, the survival rate of the mutant mice diminished markedly by four weeks after birth, and all *Atg7*$^{flox/flox}$; nestin-*Cre* mice were dead within 28 weeks (Fig. 1b). We also observed growth retardation as early as P14 in these mice (data not shown). Furthermore, the mice showed motor and behavioural deficits, including abnormal limb-clasping reflexes (Fig. 1c) and tremor, and in some cases, they walked on their tiptoes. In a rotarod test, most *Atg7*$^{flox/flox}$; nestin-*Cre* mice fell after grasping the rod only briefly (Fig. 1d). These motor and behavioural deficits began to appear at P14–P21. These results suggest that autophagy deficiency in the central nervous system results in a severe neurological disorder.

Histological analysis using Meyer's haematoxylin and eosin (H&E) staining showed marked atrophy of the cerebral cortical region of *Atg7*$^{flox/flox}$; nestin-*Cre* brain at P56 (Fig. 2a, b). The ratios of cortical thickness to dorsoventral thickness of the brain in *Atg7*$^{flox/+}$; nestin-*Cre* and *Atg7*$^{flox/flox}$; nestin-*Cre* mice were 0.17 ± 0.00031 and 0.15 ± 0.00034, respectively ($n = 5$, $P < 0.01$). Notably, almost no large pyramidal neurons were observed in *Atg7*$^{flox/flox}$; nestin-*Cre* mice compared with the corresponding region in brains from control mice (Fig. 2c, d). Immunostaining for the glial marker GFAP (glial fibrillary acidic protein) showed an increase in GFAP signal in the cerebral cortex of *Atg7*$^{flox/flox}$; nestin-*Cre* mice (Fig. 2e, f), suggesting the presence of neuronal damage in this region. In the cerebellar

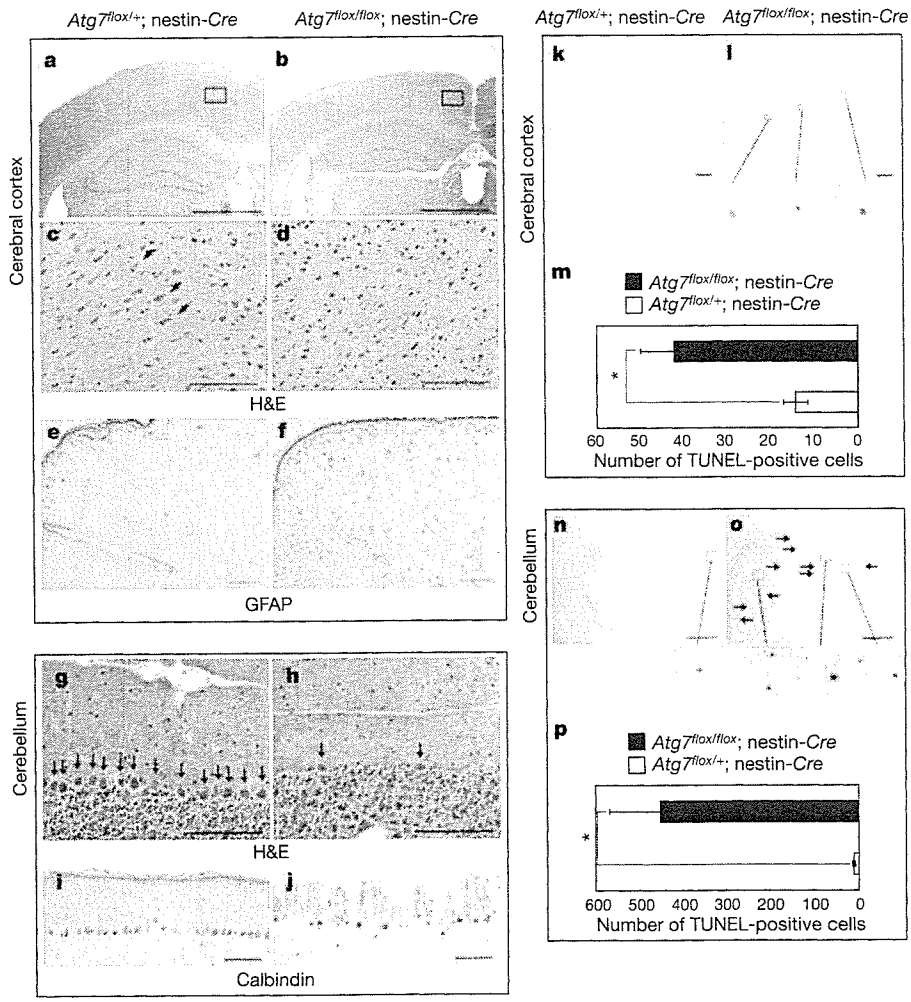

Figure 2 | Marked cell death in autophagy-deficient cerebral cortex and cerebellum. a–f, Histological analyses of *Atg7*$^{flox/+}$; nestin-*Cre* (left) and *Atg7*$^{flox/flox}$; nestin-*Cre* (right) cerebral cortex at P56. Cryosections were stained with H&E (**a–d**) or immunostained for the glial marker GFAP (**e**, **f**). Boxed areas in **a** and **b** are magnified in **c** and **d**, respectively. Arrows in **c** point to large pyramidal neurons in the cerebral cortex. **g–j**, Histological analysis of *Atg7*$^{flox/+}$; nestin-*Cre* (left) and *Atg7*$^{flox/flox}$; nestin-*Cre* (right) cerebellum at P56. Cryosections were stained with H&E (**g**, **h**) or immunostained for the Purkinje marker calbindin (**i**, **j**). Arrows in **g** and **h** indicate cerebellar Purkinje cells. **k–p**, TUNEL staining of the cerebral cortex (**k**, **l**) and cerebellum (**n**, **o**) at P56 in *Atg7*$^{flox/+}$; nestin-*Cre* (**k**, **n**) and *Atg7*$^{flox/flox}$; nestin-*Cre* (**l**, **o**) sections. TUNEL-positive cells are indicated with arrows and shown as higher magnification images beneath panels **l**, **n** and **o**. Histograms show the average number (±s.d.) of TUNEL-positive cells in ten sections for three animals of each genotype (**m**, **p**). *, $P < 0.05$ (*t*-test). Scale bars, 1 mm (**a**, **b**), 100 μm (**c–j**), 250 μm (**k**, **l**, **n**, **o**). We observed no sex difference in brain morphology or neuronal loss in *Atg7*$^{flox/flox}$; nestin-*Cre* mice.

cortex, H&E staining revealed a large reduction in the number of Purkinje cells in the mutant brain (Fig. 2g, h), which was further confirmed by immunolabelling of Purkinje cells with an anti-calbindin antibody (Fig. 2i, j). Similar neuronal loss was also recognized in the hippocampal pyramidal cell layer of mutant brain (Supplementary Fig. S2).

To determine whether the reduced number of neurons observed in *Atg7*$^{flox/flox}$; nestin-*Cre* mouse brain was caused by cell death, we performed TUNEL (TdT-mediated dUTP nick end labelling) assays. We observed a marked increase in the number of TUNEL-positive cells in the cerebral cortex (Fig. 2k–m) and granular cell layer of the cerebellum at P56 in *Atg7*$^{flox/flox}$; nestin-*Cre* mice (Fig. 2n–p) compared with control mouse brains. Although loss of Purkinje cells was observed in the mutant brain, we could not detect TUNEL-positive Purkinje cells at any developmental stage examined. However, when *Atg7* was specifically depleted in Purkinje cells using transgenic mice expressing Cre recombinase under the control of the *Pcp2* gene promoter (Pcp2-*Cre*), a marked reduction in the number of Purkinje cells was detected in the absence of TUNEL reactivity (data not shown), suggesting that neurons deficient in autophagy can die in a cell-autonomous fashion. Together, these results indicate that lack of autophagy in the central nervous system leads to neurodegeneration.

We have previously reported that autophagy is responsible for constitutive protein turnover in quiescent hepatocytes even under nutrient-rich conditions, and that a defect in autophagy leads to the accumulation of large, ubiquitin-containing inclusion bodies[8]. We therefore probed brain sections with an anti-ubiquitin antibody to examine the presence of ubiquitin-containing inclusion bodies. At P56, ubiquitin-positive dots were detected in several regions of the *Atg7*$^{flox/flox}$; nestin-*Cre* mouse brain, including the cerebral cortex (Fig. 3b), cerebellar Purkinje cells (Fig. 3d), hippocampal pyramidal neurons (Fig. 3f), thalamus (data not shown), hypothalamus (Fig. 3h), amygdala (Fig. 3j) and pontine nuclei (Fig. 3l). The degree of staining varied by region. For example, whereas most neuronal

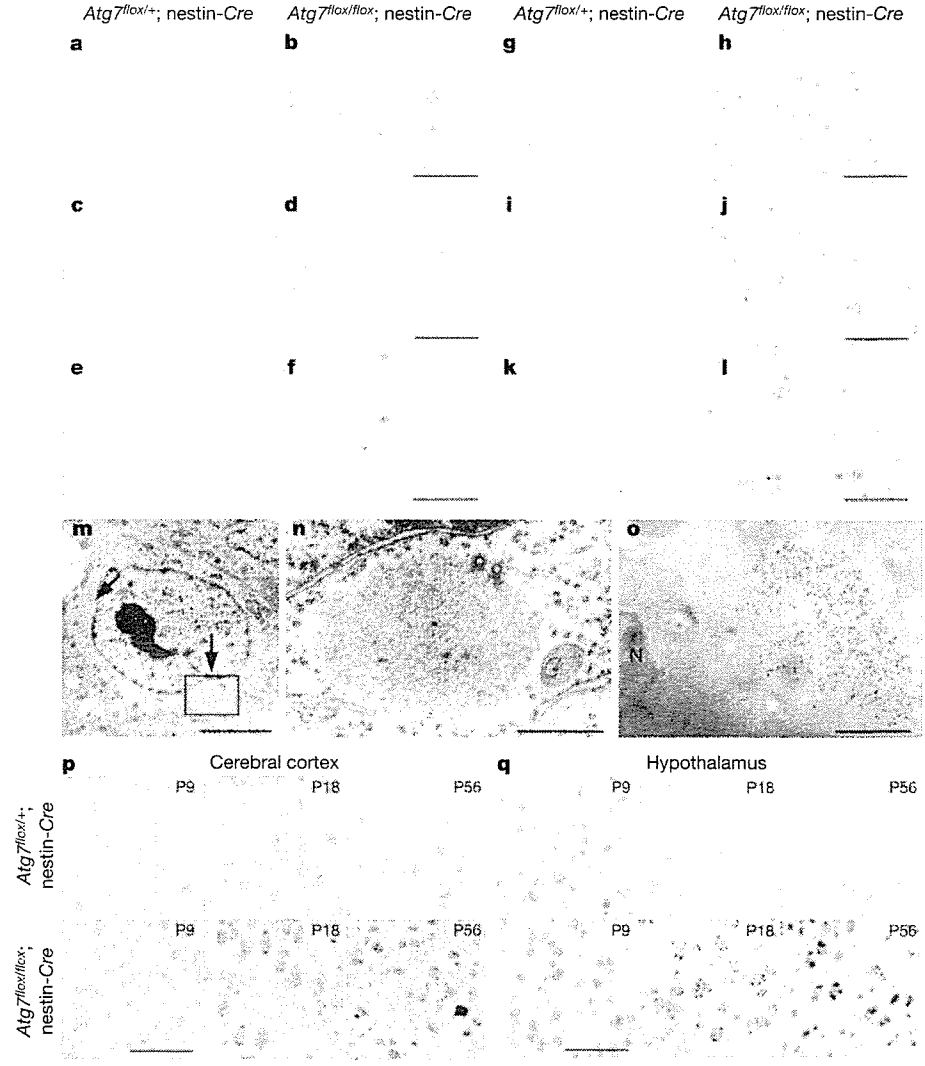

Figure 3 | Appearance of ubiquitin-positive inclusions in autophagy-deficient neurons. a–l, The presence of ubiquitin-positive dots was examined immunohistochemically in several regions including cerebral cortex (**a**, **b**), cerebellum (**c**, **d**), hippocampus (**e**, **f**), hypothalamus (**g**, **h**), amygdala (**i**, **j**) and pontine nuclei (**k**, **l**) of *Atg7*$^{flox/+}$; nestin-*Cre* and *Atg7*$^{flox/flox}$; nestin-*Cre* mice. Note the presence of numerous ubiquitin dots in the amygdala and hypothalamus of the representative mutants. Scale bars, 50 μm. **m**, **n**, Electron micrographs of the brain of *Atg7*$^{flox/flox}$; nestin-*Cre* mice. Inclusion bodies (arrows) were often observed in *Atg7*$^{flox/flox}$; nestin-*Cre* hypothalamus. The boxed region in **m** is shown in **n**. Inclusion bodies were not detected in *Atg7*$^{flox/+}$; nestin-*Cre* brain (data not shown). Scale bars, 5 μm (**m**), 1 μm (**n**). **o**, Immunoelectron micrograph of ubiquitin in a representative *Atg7*$^{flox/flox}$; nestin-*Cre* hypothalamus. N, nucleus. Scale bar, 1 μm. **p**, **q**, Immunohistochemical detection of ubiquitin-positive inclusions in the cerebral cortex (**p**) and hypothalamus (**q**) at P9, P18 and P56. Brain sections of each genotype at the indicated ages were immunostained with an anti-ubiquitin antibody. Ubiquitin-positive inclusions appeared at P18 and became larger with ageing in the brain of *Atg7*$^{flox/flox}$; nestin-*Cre* mice. Scale bars, 50 μm.

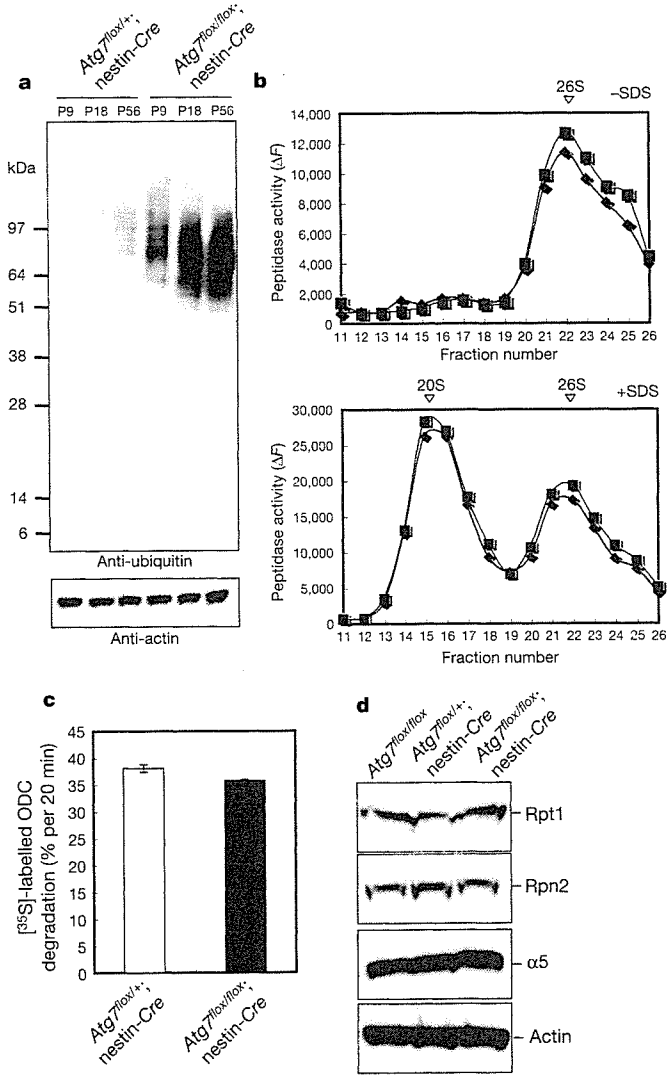

Figure 4 | Qualitative and quantitative analyses of proteasomes in autophagy-deficient brain. **a**, Increase in ubiquitinated proteins in *Atg7*$^{flox/flox}$; nestin-*Cre* mouse brain over time. Homogenates of P9, P18 and P56 brains from *Atg7*$^{flox/+}$; nestin-*Cre* and *Atg7*$^{flox/flox}$; nestin-*Cre* mice were immunoblotted with an anti-ubiquitin antibody. An anti-actin antibody was used as a loading control. Data shown are representative of three separate experiments. We observed no sex difference in the accumulation of ubiquitin in *Atg7*$^{flox/flox}$; nestin-*Cre* mice. **b**, Peptide hydrolysis activity of 20S and 26S proteasomes. Homogenates from P28 *Atg7*$^{flox/+}$; nestin-*Cre* (blue) and *Atg7*$^{flox/flox}$; nestin-*Cre* (pink) brains were fractionated by glycerol density gradient centrifugation (10–40% glycerol from fraction 1 to fraction 30). Aliquots from each fraction were used for the assay of chymotryptic activity of proteasomes using Suc-LLVY-AMC as a substrate in the absence (top) or presence (bottom) of 0.05% SDS. The sedimenting positions of 20S and 26S proteasomes are indicated with arrowheads. Note that whereas 26S proteasomes exist in active forms in tissues, 20S proteasomes are latent and are activated artificially by a low concentration of SDS. **c**, ATP-dependent degradation of [^{35}S]-labelled ODC. Degradation of [^{35}S]-labelled ODC was assayed using crude extracts from P28 *Atg7*$^{flox/+}$; nestin-*Cre* and *Atg7*$^{flox/flox}$; nestin-*Cre* brains. The experiment was repeated three times, and values represent mean ± s.d. In the above assays, there were no significant differences between *Atg7*$^{flox/+}$; nestin-*Cre* and *Atg7*$^{flox/flox}$; nestin-*Cre* mice. **d**, Immunoblot analysis of 26S proteasome components. Homogenates from P28 *Atg7*$^{flox/flox}$, *Atg7*$^{flox/+}$; nestin-*Cre* and *Atg7*$^{flox/flox}$; nestin-*Cre* brains were immunoblotted with antibodies against the indicated proteins. Data shown are representative of three separate experiments. There was no change in proteasome status for the different genotypes.

cells in the amygdala (Fig. 3j) and hypothalamus (Fig. 3h) contained several ubiquitin dots of small to large size, only a small number of cerebellar Purkinje cells stained for ubiquitin, and the immunoreactive dots were of small size (Fig. 3d). Electron microscopy showed that *Atg7*$^{flox/flox}$; nestin-*Cre* hypothalamic neurons had circular or elliptical large structures composed of fibrillar elements in the perikarya (Fig. 3m, n). Immunoelectron microscopy further confirmed that these aberrant structures contained ubiquitin (Fig. 3o). These ubiquitin dots appeared not only in the perikarya of neurons, but also in the intercellular space (see Fig. 3h, j, l). Dots found in the intercellular space might correspond to ubiquitin inside neurites, because they were observed in myelinated axons around pontine nuclei using both light and electron microscopy (Supplementary Fig. S3a, b). In contrast, almost no ubiquitin dots were observed in astroglial cells (Supplementary Fig. S3c). Together with the results in Fig. 3, we concluded that most of the distinct ubiquitin dots were located in neurons.

We examined the development of ubiquitin-containing inclusion bodies at different stages by dissecting the brains of *Atg7*$^{flox/+}$; nestin-*Cre* and *Atg7*$^{flox/flox}$; nestin-*Cre* mice at P9, P18 and P56. Only a few ubiquitin-positive aggregates were noted in the neurons of control and mutant cerebral cortex and hypothalamus at P9 (Fig. 3p, q). In contrast, several ubiquitin-containing inclusions were clearly noted in *Atg7*$^{flox/flox}$; nestin-*Cre* cortex and hypothalamus at P18, increasing in number and size by P56 (Fig. 3p, q). These results indicate an age-dependent increase in ubiquitin-containing inclusion bodies in autophagy-deficient neurons. Consistent with the above immunohistochemical analysis (Fig. 3p, q), immunoblot analysis revealed increasing levels of high-molecular-mass polyubiquitinated proteins with age in the brains of *Atg7*$^{flox/flox}$; nestin-*Cre* mice (Fig. 4a), and an increase in their insoluble forms at later developmental stages (data not shown).

Finally, we examined whether autophagy deficiency influences proteasome functions. The chymotryptic activities of 26S and 20S proteasomes (measured using Suc-LLVY-MCA as a substrate) were comparable in extracts from both control and *Atg7*$^{flox/flox}$; nestin-*Cre* brains (Fig. 4b). Furthermore, the ATP-dependent degradation of ornithine decarboxylase (ODC) by 26S proteasomes was similar in control and mutant brains (Fig. 4c). Moreover, the relative amounts of several subunits of the 26S proteasome did not change in the brain irrespective of autophagy deficiency (as detected by immunoblotting, Fig. 4d). These results indicate that age-dependent accumulation of ubiquitin-positive aggregates in the autophagy-deficient brain occurs despite the apparently normal function of proteasomes.

Over the past decade, researchers working in the field of neurodegenerative diseases have made great progress in uncovering the mechanisms of these disorders by focusing on the interplay between proteolytic stress and neural cell death[17,18]. Increasing evidence indicates that ubiquitin-positive inclusion bodies—the pathological hallmark of various neurodegenerative diseases—are formed by dysfunction of proteasome degrading machinery[3]. Indeed, proteins with aberrant structure impair proteasome functions directly, thus attenuating 'garbage disposal'[19]. On the other hand, the accumulation of autophagosomes owing to impairment of fusion with lysosomes is observed in various disorders, including Alzheimer's disease[20–22], and it has been proposed that autophagy functions to degrade toxic proteins in familial neurodegenerative diseases[23–25]. However, it remains unknown whether these two proteolytic systems work independently or cooperatively to maintain protein homeostasis in cells. Furthermore, whether autophagy has a role in cell death or cell survival is currently under debate[26].

We have shown that *Atg7*$^{flox/flox}$; nestin-*Cre* mice exhibit neurological abnormalities and neuronal death, suggesting that impaired autophagy causes neurodegeneration. We suggest a particularly important role for autophagy in the brain, to which nutrients must be constantly supplied from other organs, even under fasting conditions. Moreover, we find that autophagy deficiency in neurons leads to the accumulation of ubiquitin-containing inclusion bodies,

without obvious deficits in proteasome function. Hence, our data indicate a central role for constitutive autophagy in the elimination of unfavourable proteins and in the survival of neurons, independent of the proteasome system (see the proposed model in Supplementary Fig. S4). Although we do not know whether autophagy and proteasome degradation target a similar set of normal and/or misfolded proteins, it is plausible that the autophagic pathway assists in degrading accumulated intractable proteins when cellular levels of aberrant proteins overwhelm the disposal capacity of the proteasome.

We have shown that a lack of autophagy is associated with neurodegeneration, even in the absence of harmful gene products found in neurodegenerative disorders such as Huntington's disease, Parkinson's disease and amyotrophic lateral sclerosis. We therefore predict that the role of autophagy becomes even more critical in the pathogenesis of such neurodegenerative diseases, when disease-related, aggregation-prone proteins are expressed as a result of genetic mutations and/or environmental insults, leading to early-onset symptoms.

METHODS

Animals. Nestin-*Cre* transgenic mice[14] were purchased from the Jackson Laboratory. $Atg7^{flox/flox}$ mice[8] were bred with nestin-*Cre* transgenic mice to produce $Atg7^{flox/flox}$; nestin-*Cre* mice. Mice were housed in a pathogen-free facility. Motor function was assessed using a rotarod test[27]. Experimental protocols were approved by the Ethics Review Committee for Animal Experimentation at the Tokyo Metropolitan Institute of Medical Science.

Immunoblot analysis. Immunoblots were carried out as described previously[8]. Antibodies against Atg7, Atg5 and LC3 have been described previously[8]. Antibodies against Rpt1, Rpn2 and α5 were provided by K. B. Hendil. Polyclonal anti-ubiquitin (FK2; Medical & Biological Laboratories) and anti-actin (MAB1501R; Chemicon) antibodies were also used.

Histological examination. $Atg7^{flox/+}$; nestin-*Cre* and $Atg7^{flox/flox}$; nestin-*Cre* mice were fixed by cardiac perfusion with 0.1 M phosphate buffer containing 4% paraformaldehyde, 4% sucrose for light microscopy and immunohistochemistry, with 0.1 M phosphate buffer containing 2% paraformaldehyde, 2% glutaraldehyde for standard electron microscopy, or with 0.1 M phosphate buffer containing 4% paraformaldehyde, 0.1% glutaraldehyde for immunoelectron microscopy. Brain tissues were excised and processed for morphological analysis as described previously[8,28]. For light microscopic analysis, 10-μm cryosections were cut and stained with H&E or immunolabelled with the following antibodies: anti-human NeuN (Abcam), anti-GFAP (Sigma), anti-calbindin (Sigma), anti-myelin basic protein (MBP; MCA409S, Serotec) and anti-ubiquitin (DAKO) antibodies. The TUNEL assay has been described previously[28]. For counting TUNEL-positive signals in the cerebral cortex, 60 coronal sections containing the anterior portion of the hippocampus (~0.6-mm thick in total) were cut, and TUNEL staining was performed on every sixth section, on a total of ten sections.

Electron microscopy and immunoelectron microscopy. Fixed brains were post-fixed with 1% OsO_4, embedded in Epon812 and sectioned. Immunoelectron microscopy was carried out on cryothin sections as described previously[29]. In brief, brains were frozen in phosphate buffer containing 2.3 M sucrose and 20% polyvinyl pyrrhoridon. Ultrathin sections were mounted on Formvar carbon-coated nickel grids, blocked with 1% bovine serum albumin (BSA) in PBS, and incubated with anti-ubiquitin antibody (1B3) and colloidal gold-conjugated secondary antibody.

Glycerol gradient analysis. Samples were fractionated by 10–40% (v/v) linear glycerol density gradient centrifugation (22 h, 100,000*g*) as described previously[30].

Assay of proteasome activity. Peptidase activity was measured using a fluorescent peptide substrate, succinyl-Leu-Leu-Val-Tyr-7-amido-4-methylcoumarin (Suc-LLVY-MCA), as described previously[30]. Ornithine decarboxylase (ODC)-degradation activity was assayed as described previously[30].

Received 6 February; accepted 20 March 2006.
Published online 19 April 2006.

1. Forman, M. S., Trojanowski, J. Q. & Lee, V. M. Neurodegenerative diseases: a decade of discoveries paves the way for therapeutic breakthroughs. *Nature Med.* 10, 1055–1063 (2004).
2. Shintani, T. & Klionsky, D. J. Autophagy in health and disease: a double-edged sword. *Science* 306, 990–995 (2004).
3. Goldberg, A. L. Protein degradation and protection against misfolded or damaged proteins. *Nature* 426, 895–899 (2003).
4. Reggiori, F. & Klionsky, D. J. Autophagosomes: biogenesis from scratch? *Curr. Opin. Cell Biol.* 17, 415–422 (2005).
5. Levine, B. & Klionsky, D. J. Development by self-digestion: molecular mechanisms and biological functions of autophagy. *Dev. Cell* 6, 463–477 (2004).
6. Tsukada, M. & Ohsumi, Y. Isolation and characterization of autophagy-defective mutants of *Saccharomyces cerevisiae*. *FEBS Lett.* 333, 169–174 (1993).
7. Kuma, A. *et al.* The role of autophagy during the early neonatal starvation period. *Nature* 432, 1032–1036 (2004).
8. Komatsu, M. *et al.* Impairment of starvation-induced and constitutive autophagy in *Atg7*-deficient mice. *J. Cell Biol.* 169, 425–434 (2005).
9. Melendez, A. *et al.* Autophagy genes are essential for dauer development and life-span extension in *C. elegans*. *Science* 301, 1387–1391 (2003).
10. Juhasz, G., Csikos, G., Sinka, R., Erdelyi, M. & Sass, M. The *Drosophila* homolog of Aut1 is essential for autophagy and development. *FEBS Lett.* 543, 154–158 (2003).
11. Paludan, C. *et al.* Endogenous MHC class II processing of a viral nuclear antigen after autophagy. *Science* 307, 593–596 (2005).
12. Nakagawa, I. *et al.* Autophagy defends cells against invading group A *Streptococcus*. *Science* 306, 1037–1040 (2004).
13. Gutierrez, M. G. *et al.* Autophagy is a defense mechanism inhibiting BCG and *Mycobacterium tuberculosis* survival in infected macrophages. *Cell* 119, 753–766 (2004).
14. Betz, U. A., Vosshenrich, C. A., Rajewsky, K. & Muller, W. Bypass of lethality with mosaic mice generated by Cre–*loxP*-mediated recombination. *Curr. Biol.* 6, 1307–1316 (1996).
15. Ohsumi, Y. Molecular dissection of autophagy: two ubiquitin-like systems. *Nature Rev. Mol. Cell Biol.* 2, 211–216 (2001).
16. Kabeya, Y. *et al.* LC3, a mammalian homologue of yeast Apg8p, is localized in autophagosome membranes after processing. *EMBO J.* 19, 5720–5728 (2000).
17. Ciechanover, A. & Brundin, P. The ubiquitin proteasome system in neurodegenerative diseases: sometimes the chicken, sometimes the egg. *Neuron* 40, 427–446 (2003).
18. Bossy-Wetzel, E., Schwarzenbacher, R. & Lipton, S. A. Molecular pathways to neurodegeneration. *Nature Med.* 10 (Suppl.), S2–S9 (2004).
19. Bence, N. F., Sampat, R. M. & Kopito, R. R. Impairment of the ubiquitin-proteasome system by protein aggregation. *Science* 292, 1552–1555 (2001).
20. Yu, W. H. *et al.* Macroautophagy–a novel β-amyloid peptide-generating pathway activated in Alzheimer's disease. *J. Cell Biol.* 171, 87–98 (2005).
21. Tanaka, Y. *et al.* Accumulation of autophagic vacuoles and cardiomyopathy in LAMP-2-deficient mice. *Nature* 406, 902–906 (2000).
22. Nishino, I. *et al.* Primary LAMP-2 deficiency causes X-linked vacuolar cardiomyopathy and myopathy (Danon disease). *Nature* 406, 906–910 (2000).
23. Webb, J. L., Ravikumar, B., Atkins, J., Skepper, J. N. & Rubinsztein, D. C. α-Synuclein is degraded by both autophagy and the proteasome. *J. Biol. Chem.* 278, 25009–25013 (2003).
24. Ravikumar, B. *et al.* Inhibition of mTOR induces autophagy and reduces toxicity of polyglutamine expansions in fly and mouse models of Huntington disease. *Nature Genet.* 36, 585–595 (2004).
25. Fortun, J., Dunn, W. A. Jr, Joy, S., Li, J. & Notterpek, L. Emerging role for autophagy in the removal of aggresomes in Schwann cells. *J. Neurosci.* 23, 10672–10680 (2003).
26. Levine, B. & Yuan, J. Autophagy in cell death: an innocent convict? *J. Clin. Invest.* 115, 2679–2688 (2005).
27. Bontekoe, C. J. *et al.* Knockout mouse model for *Fxr2*: a model for mental retardation. *Hum. Mol. Genet.* 11, 487–498 (2002).
28. Koike, M. *et al.* Involvement of two different cell death pathways in retinal atrophy of cathepsin D-deficient mice. *Mol. Cell. Neurosci.* 22, 146–161 (2003).
29. Waguri, S. *et al.* Cysteine proteinases in GH4C1 cells, a rat pituitary tumour cell line, are secreted by the constitutive and regulated secretory pathways. *Eur. J. Cell Biol.* 67, 308–318 (1995).
30. Tanahashi, N. *et al.* Hybrid proteasomes. Induction by interferon-γ and contribution to ATP-dependent proteolysis. *J. Biol. Chem.* 275, 14336–14345 (2000).

Supplementary Information is linked to the online version of the paper at www.nature.com/nature.

Acknowledgements We thank T. Kaneko, T. Kouno and K. Tatsumi for technical assistance. We also thank A. Yabashi, K. Kanno, F. Kaji and K. Ikeue for help with morphological analysis, J. Ezaki for discussion, and Z. Yue for critical reading of the manuscript. This work was supported in part by a Grant-in-Aid from the Ministry of Education, Culture, Sports, Science and Technology of Japan.

Author contributions M.K. and T.C. generated $Atg7^{flox/flox}$ mice, and M.K. and J.I. performed most of the experiments to characterize $Atg7^{flox/flox}$; nestin-*Cre* mice. S.W. performed histological and microscopic analyses, and S.M. performed the biochemical analysis of proteasome activity. M.K., S.W. and K.T. wrote the paper. All authors discussed the results and commented on the manuscript.

Author Information Reprints and permissions information is available at npg.nature.com/reprintsandpermissions. The authors declare no competing financial interests. Correspondence and requests for materials should be addressed to K.T. (tanakak@rinshoken.or.jp).

The EMBO Journal (2006) 25, 4524–4536 | © 2006 European Molecular Biology Organization | All Rights Reserved 0261-4189/06
www.embojournal.org

THE EMBO JOURNAL

A novel proteasome interacting protein recruits the deubiquitinating enzyme UCH37 to 26S proteasomes

Jun Hamazaki[1,2], Shun-ichiro Iemura[3], Tohru Natsume[3], Hideki Yashiroda[1], Keiji Tanaka[1] and Shigeo Murata[1,4,*]

[1]Laboratory of Frontier Science, Core Technology and Research Center, Tokyo Metropolitan Institute of Medical Science, Bunkyo-ku, Tokyo, Japan, [2]Department of Biological Sciences, Graduate School of Science, Tokyo Metropolitan University, Hachiohji, Tokyo, Japan, [3]National Institutes of Advanced Industrial Science and Technology, Biological Information Research Center, Kohtoh-ku, Tokyo, Japan and [4]PRESTO, Japan Science and Technology Agency, Kawaguchi, Saitama, Japan

The 26S proteasome is a multisubunit protease responsible for regulated proteolysis in eukaryotic cells. It is composed of one catalytic 20S proteasome and two 19S regulatory particles attached on both ends of 20S proteasomes. Here, we describe the identification of Adrm1 as a novel proteasome interacting protein in mammalian cells. Although the overall sequence of Adrm1 has weak homology with the yeast Rpn13, the amino- and carboxyl-terminal regions exhibit significant homology. Therefore, we designated it as hRpn13. hRpn13 interacts with a base subunit Rpn2 via its amino-terminus. The majority of 26S proteasomes contain hRpn13, but a portion of them does not, indicating that hRpn13 is not an integral subunit. Intriguingly, we found that hRpn13 recruits UCH37, a deubiquitinating enzyme known to associate with 26 proteasomes. The carboxyl-terminal regions containing KEKE motifs of both hRpn13 and UCH37 are involved in their physical interaction. Knockdown of hRpn13 caused no obvious proteolytic defect but loss of UCH37 proteins and decrease in deubiquitinating activity of 26S proteasomes. Our results indicate that hRpn13 is essential for the activity of UCH37.

The EMBO Journal (2006) **25,** 4524–4536. doi:10.1038/sj.emboj.7601338; Published online 21 September 2006
Subject Categories: proteins
Keywords: deubiquitinating enzyme; proteasome; Rpn13; ubiquitin; UCH37

Introduction

The ubiquitin–proteasome system is the main non-lysosomal route for intracellular protein degradation in eukaryotes (Glickman and Ciechanover, 2002). Short-lived proteins as well as abnormal proteins in cells are recognized by the ubiquitin system and are marked with ubiquitin chains as a degradation signal. Polyubiquitinated proteins are then recognized and degraded by 26S proteasomes. The 26S proteasome is a huge protein complex of approximately 2.5 MDa composed of one proteolytically active 20S proteasome and two 19S regulatory particles (RP), each attached to one end of the 20S proteasome (Baumeister *et al*, 1998). The 20S proteasome is a barrel-shaped complex formed by the axial stacking of four rings made up of two outer α-rings and two inner β-rings, which are each made up of seven structurally similar α- and β-subunits, respectively, being associated in the order of $\alpha_{1-7}\beta_{1-7}\beta_{1-7}\alpha_{1-7}$ (Coux *et al*, 1996). The interior of the cavity composed of β-rings is responsible for its proteolytic activity. However, the entry of substrates into the cavity of 20S proteasomes is restricted by the narrow gate of α-rings, which is closed in itself. The 19S RP plays an important role in the degradation of ubiquitinated proteins. The 19S RP can be divided into two subcomplexes, known as 'base' and 'lid' (Glickman *et al*, 1998). The base is made up of six ATPases (Rpt1–Rpt6) and two large regulatory components, Rpn1 and Rpn2, functioning as presumptive receptor(s) of ubiquitin-like proteins (Leggett *et al*, 2002), whereas the lid contains multiple non-ATPase subunits (Rpn3, Rpn5–9, Rpn11–13, and Rpn15). The base complex binds to the outer α-ring of the 20S proteasome and opens a narrow gate in an ATP-dependent manner (Smith *et al*, 2005). In addition, the ATPase subunits supply energy for unfolding target proteins, so that they can be translocated into the β-ring cavity of 20S proteasomes where active sites are located. The role of the lid complex is less unraveled. Among the lid subunits, Rpn11 is known as a metalloprotease that cleaves the peptide bonds between the substrate and the most proximal ubiquitin of the polyubiquitin chains (Verma *et al*, 2002; Yao and Cohen, 2002). Rpn10 is thought to lie between the base and the lid complex and serve as one of the ubiquitin receptors (Verma *et al*, 2004).

In addition to the genuine proteasome subunits, several molecules that associate with proteasomes and play auxiliary roles have been identified (Verma *et al*, 2000; Leggett *et al*, 2002). Most of the proteasome studies have been carried out using yeast cells, especially budding yeasts, and less is known about mammalian proteasomes and some of the counterparts of yeast proteasome subunits have not yet been identified. Here, we show that Adrm1, which was previously reported as a membrane glycoprotein (Shimada *et al*, 1991, 1994), is an ortholog of yeast Rpn13 and identify it as a novel interacting protein of mammalian 26S proteasomes. Furthermore, we reveal that it recruits UCH37, a deubiquitinating enzyme (DUB) associated with proteasomes (Lam *et al*, 1997; Li *et al*, 2000; Stone *et al*, 2004).

Results

Adrm1 is a mammalian ortholog of yeast Rpn13

To identify proteins involved with mammalian proteasomes, we searched for cellular proteins that physically associate,

*Corresponding author. Laboratory of Frontier Science, Core Technology and Research Center, Tokyo Metropolitan Institute of Medical Science, 3-18-22 Honkomagome, Bunkyo-ku, Tokyo 113-9613, Japan.
Tel./Fax: +81 3 3823 2237; E-mail: smurata@rinshoken.or.jp

Received: 21 February 2006; accepted: 15 August 2006; published online: 21 September 2006

directly or indirectly, with 26S proteasomes in mammalian cells. For this purpose, the human ortholog of Rpn10 (hRpn10: hereafter, 'h' is used as a prefix to indicate a human ortholog of any yeast proteasome subunit) with a carboxyl-terminal Flag tag was expressed in HEK293 cells and immunoprecipitated from cell lysates with anti-Flag antibody. The immunoprecipitates were eluted with Flag peptides, digested with Lys-C endopeptidase, and analyzed using a highly sensitive direct nano-flow liquid chromatography/tandem mass spectrometry (LC–MS/MS) (Natsume *et al*, 2002). Following a database search, 30 peptides were assigned to MS/MS spectra for Flag-hRpn10-associated complexes (Supplementary Figure 1). These data identified almost all the subunits of 26S proteasomes. In addition, we identified a molecule with yet unknown relevance to proteasomes, called Adrm1.

Adrm1 was previously reported as a membrane glycoprotein with a molecular mass of 110 kDa and involved in cell adhesion (Shimada *et al*, 1994; Simins *et al*, 1999; Natsume *et al*, 2002). Exploration of the Proteome BioKnowledge Library (https://www.proteome.com/proteome/Retriever/index.html) database indicated that Adrm1 is weakly homologous to Rpn13, a subunit of budding yeast proteasomes (Verma *et al*, 2000). The overall sequence of Adrm1 showed 24.9% homology with that of Rpn13, whereas it exhibited a high homology of 60.2% with the amino-termini of Adrm1 (residues 22–111) and Rpn13 (residues 7–103). We also identified 74.4% homology between the C-termini of Adrm1 (residues 366–407) and Rpn13 (residues 114–156) (Figure 1). Accordingly, we renamed the molecule hRpn13.

Identification of hRpn13 as a novel proteasome interacting protein in mammals

To verify that hRpn13 is a human counterpart of yeast Rpn13, we tested whether hRpn13 is incorporated into 26S proteasomes. Extracts of 293T cells were fractionated by glycerol gradient centrifugation, and each fraction was subjected to immunoblotting with anti-hRpn13 antibody. Almost all hRpn13 proteins co-sedimented with 26S proteasomes that were detected by succinyl-Leu-Leu-Val-Tyr-7-amido-4-methylcoumarin (Suc-LLVY-MCA)-hydrolyzing activity and sedimentation of a genuine proteasome subunit hRpn1 (Figure 2A). Free forms of hRpn13 were not apparently observed (Figure 2A). 26S proteasomes were further purified from fractions 18–20 by immunoprecipitation using anti-hRpt6 antibody, and then the immunoprecipitates were subjected to two-dimensional polyacrylamide gel electrophoresis (2D-PAGE). Immunoblot for hRpn13 detected a spot that had an isoelectric point (p*I*) and molecular mass that corresponded to the predicted values of p*I* 4.8 and 42.1 kDa, respectively (Figure 2B). Tandem mass spectrometric analysis identified this spot as Adrm1 (data not shown). Adrm1 has been reported as a glycosylated membrane protein with a molecular mass of 110 kDa (Shimada *et al*, 1994), which is in conflict with the notion that Adrm1, that is, hRpn13, is a subunit of proteasomes. Immunostaining of HeLa cells using anti-hRpn13 and anti-hRpn1 antibodies showed that the distribution of hRpn13 was mainly in the nucleus and partially in the cytosol, a pattern quite similar to the distribution of hRpn1 (Figure 2C). These results were in agreement with those reported previously showing that proteasomes are predominantly present in the nuclei of rapidly proliferating mammalian cells (Kumatori *et al*, 1990). Thus, in our hands, there was no evidence that hRpn13 is a membrane protein.

Next, we examined whether all 26S proteasomes contain hRpn13. The 26S proteasome fractions (fractions 18–20 in Figure 2A) were immunodepleted using anti-hRpt6 antibody, anti-hRpn13 antibody, or preimmune serum. Anti-hRpt6 antibody completely immunodepleted hRpn13 and other 19S RP

Figure 1 Sequence alignment of human Adrm1 and budding yeast Rpn13. The amino-acid sequences were aligned by the DIALIGN-T program. Amino acids that are identical, strongly similar, and weakly similar between the two sequences are boxed in black, dark gray, and light gray, respectively. Hs: *Homo sapiens*; Sc: *Saccharomyces cerevisiae*.

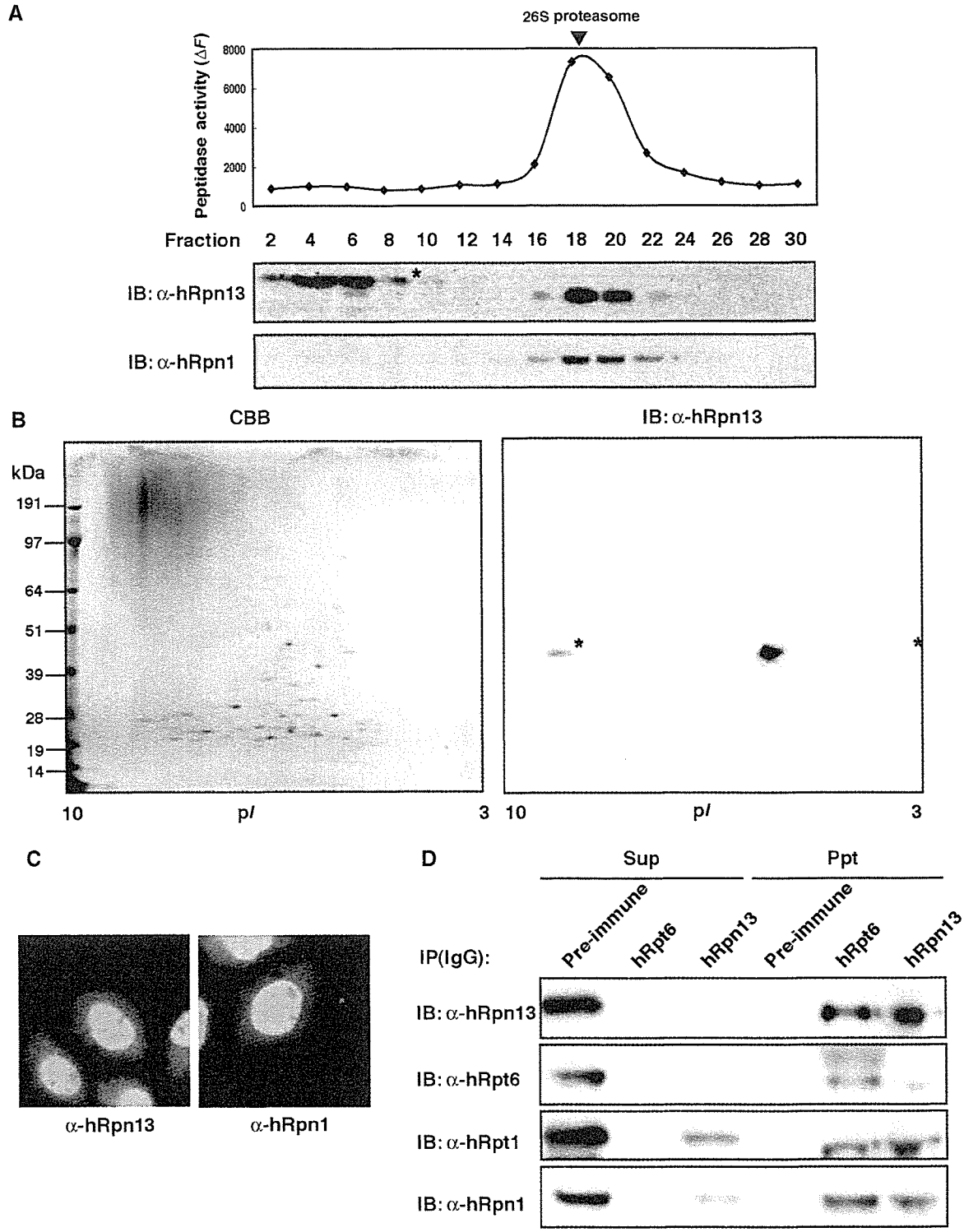

Figure 2 hRpn13 is a subunit of mammalian 26S proteasomes. (**A**) Sedimentation velocity analysis. Extracts of HEK293T cells were fractionated by 10–40% glycerol gradient centrifugation into 32 fractions from the top. An aliquot of each fraction was subjected to the assay of Suc-LLVY-MCA-hydrolyzing activity (upper panel). Immunoblot analysis of each fraction was performed using antibodies against hRpn1 and hRpn13 (lower panels). Arrowhead indicates the peak fraction of 26S proteasomes. Asterisk indicates artifact bands. (**B**) Affinity purification of human proteasomes. Fractions 18–20 in panel A were subjected to immunoprecipitation using anti-hRpt6 antibody. The precipitates were eluted with glycine–HCl and resolved by 2D-PAGE, followed by Coomassie brilliant blue (CBB) staining (left panel) and immunoblot with anti-hRpn13 antibody (right panel). (**C**) Intracellular distribution of hRpn13 in HeLa cells. hRpn13 (left panel) and hRpn1 (right panel) were detected with anti-hRpn13 or anti-hRpn1 antibody and visualized with Alexa488-conjugated anti-rabbit IgG antibody. (**D**) Immunodepletion analysis. Fractions 18–20 in panel A were pooled and immunoprecipitated with anti-hRpt6 antibody, anti-hRpn13 antibody, or preimmune serum. The unbound fractions and immunoprecipitates were subjected to SDS–PAGE, followed by immunoblotting for hRpn13, hRpt6, hRpt1, and hRpn1.

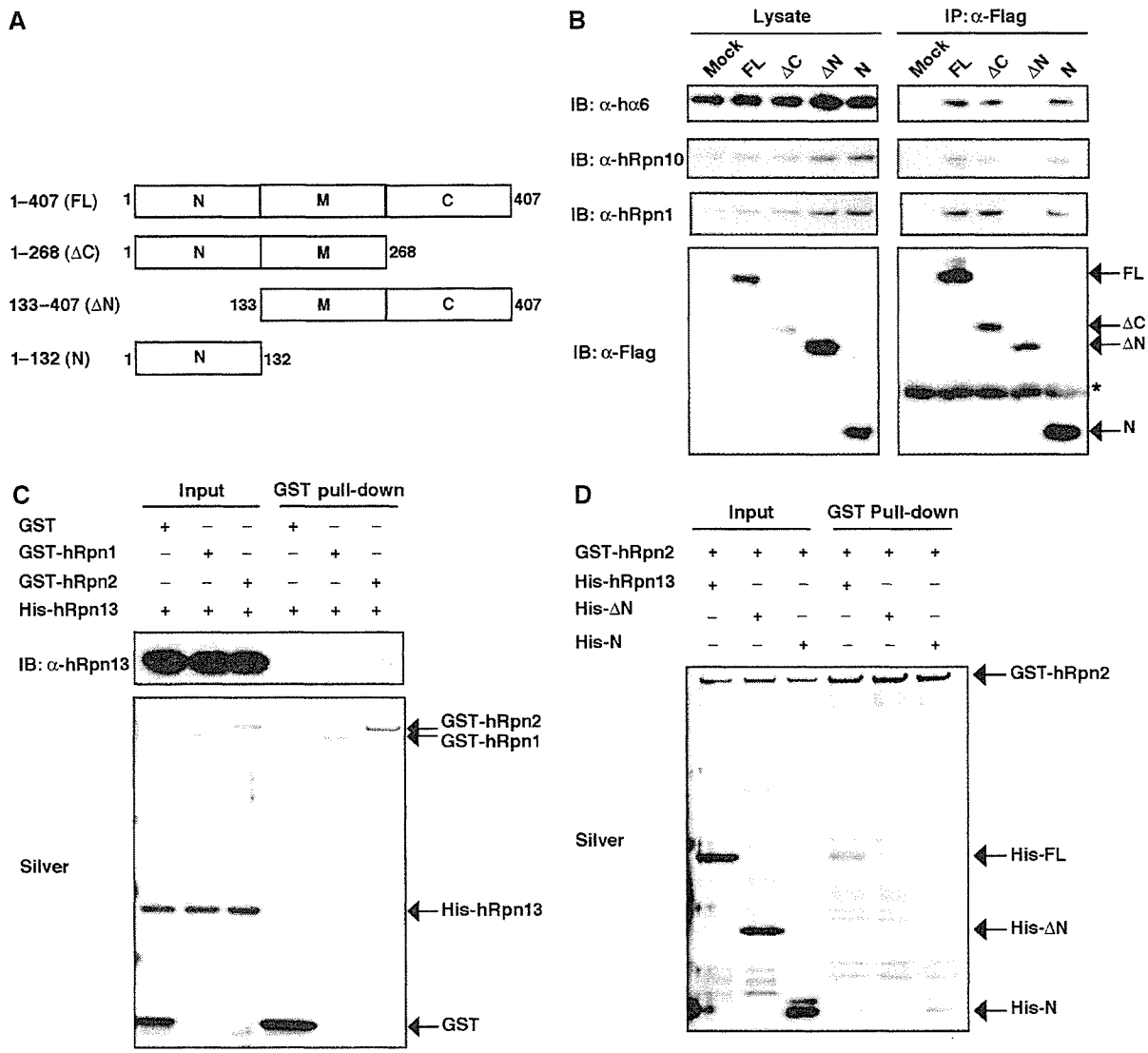

Figure 3 hRpn13 associates with proteasomes via its N-terminal region. (**A**) Schematic representation of constructs for Rpn13 and its dissected mutants used. (**B**) Flag-tagged plasmids encoding hRpn13 and its deletion mutants depicted in panel A were transfected into HEK293T cells. The cell lysates were immunoprecipitated with anti-Flag antibody, followed by immunoblotting for hα6, hRpn10, hRpn1, and Flag epitopes. (**C**) GST pull-down analysis of recombinant proteins. GST, GST-hRpn1, and GST-hRpn2 were incubated with 6xHis-hRpn13 for 1 h at 4°C and then precipitated with glutathione Sepharose. The bound proteins were analyzed by SDS–PAGE, followed by silver staining and immunoblotting with anti-hRpn13 antibody. (**D**) GST pull-down analysis of recombinant proteins. GST-hRpn2 was incubated with 6xHis-hRpn13 or its mutant forms and then pulled down with glutathione Sepharose followed by silver staining.

subunits such as hRpt1 and hRpn1. In contrast, anti-hRpn13 antibody did not remove all the 19S RP subunits, with about 10% input of 19S RP being left in the unbound fraction, whereas it completely depleted hRpn13 (Figure 2D). These results indicate that hRpn13 is incorporated into the majority of 26S proteasomes, but a portion of 26S proteasomes does not contain hRpn13. Therefore, we conclude that hRpn13 is one of the near-stoichiometric proteasome interacting proteins (PIPs), like Ubp6 and Ecm29 in budding yeast (Leggett *et al*, 2002), and is not an integral subunit of 26S proteasomes.

The conserved N-terminal region of hRpn13 is required for association with proteasomes

Based on the sequence alignment, we postulated that hRpn13 is composed of three regions. The N- and C-terminal regions are conserved between budding yeast and human, and the internal region that lies between the N- and C-terminal regions is not found in the budding yeast Rpn13 (Figure 1). We tentatively divided hRpn13 into three portions. The 'N' portion encompassed the conserved N-terminal region (i.e. amino acids 1–132) and the 'C' portion corresponded to amino acids 269–407 that included the conserved C-terminal region. The portion between 'N' and 'C' was designated 'M' portion (Figure 3A). In the next step, we determined the portion required for incorporation into proteasomes. Various deletion constructs encoding wild-type and mutant hRpn13 with Flag tag were expressed in HEK293T cells and immunoprecipitated with anti-Flag antibody. The hRpn13 mutants that lacked the C portion or encoded solely the N portion precipitated various proteasome subunits such as hα6, hRpn10, and hRpn1, as did full-length hRpn13 (Figure 3B). In contrast, hRpn13 that lacked the N portion did not precipitate these subunits (Figure 3B). These results indicate

that the N portion, that is, the conserved N-terminal region of hRpn13, is essential and sufficient for its association with proteasomes.

hRpn13 directly interacts with a base subunit hRpn2

The next set of experiments determined the subunit of 26S proteasomes associated with hRpn13. For this purpose, we tested the interaction between hRpn13 and each subunit of mammalian 19S RP by yeast two-hybrid analysis. The results identified hRpn1 and hRpn2 as possible interacting subunits with hRpn13 (data not shown). Furthermore, comprehensive interactive proteome analysis in budding yeast showed interaction of Rpn13 with Rpn2 (Ito *et al*, 2001). Therefore, we purified recombinant proteins of hRpn1, hRpn2, and hRpn13 and performed *in vitro* binding analysis (Figure 3C). hRpn13 was pulled down by glutathione *S*-transferase (GST)-hRpn2 but not by GST-hRpn1, indicating that hRpn13 is directly associated with hRpn2. Next, we tested whether the N-terminal region of hRpn13 is required for the association with hRpn2. As shown in Figure 3D, the N portion of hRpn13 was required and sufficient for interaction with GST-hRpn2, which was consistent with the results shown in Figure 3B. Based on these results, we conclude that hRpn13 is associated with 26S proteasomes via hRpn2, with which the conserved N-terminal region of hRpn13 interacts.

Knockdown of Rpn13 does not cause proteolytic defects in proteasomes

In budding yeast, deletion of Rpn13 is not lethal, unlike most other proteasome subunits, but causes defect in the degradation of a ubiquitin-fusion-degradation (UFD) substrate (Verma *et al*, 2000). To elucidate the function of hRpn13 in mammalian cells, we knocked down hRpn13 by small interfering RNA (siRNA) in HEK293T cells. As a positive control for proteasome dysfunction, knockdown of hRpt2 was also performed. In hRpt2 knockdown cells, a decrease in hRpt2 protein levels resulted in a concomitant loss of hRpn13 as well as other genuine proteasome subunits such as hRpn1 and hα6. Consequently, hRpt2-knockdown cells showed cell death (data not shown) and accumulation of polyubiquitinated proteins (Figure 4A), which are hallmarks of proteasome dysfunction. These results indicate that hRpt2 is required for the integrity of proteasome structure and function and that hRpn13 is stably expressed in the presence of normal proteasomes. In hRpn13-knockdown cells, the expression of hRpn13 was almost abrogated, but the expression of other proteasome subunits was not changed (Figure 4A). The cells showed normal growth (data not shown) and no accumulation of polyubiquitinated proteins (Figure 4A). These features were in contrast to the phenotypes of hRpt2 knockdown. When the extracts from HEK293T cells were fractionated by glycerol-density gradient centrifugation, an active enzyme that catalyzes the degradation of the fluorogenic substrate Suc-LLVY-AMC was sedimented with a sedimentation coefficient of approximately that of 26S, but low activity was found in the slowly sedimenting fractions corresponding to the sedimentation position of the purified 20S proteasome (Figure 4B, upper panel). The addition of 0.05% SDS, which is a potent artificial activator of the latent 20S proteasome, caused marked activation of the enzyme sedimenting like the 20S proteasome (Figure 4B, lower panel). As shown in Figure 4B, the peptide-hydrolyzing activities of both 20S and 26S proteasomes remained unchanged irrespective of hRpn13 knockdown. Next, we tested the activities of protein degradation *in vitro* (Figure 4C and D) and *in vivo* (Figure 4E). Assay of antizyme (AZ)-dependent ornithine decarboxylase (ODC) degradation, which measures ATP-dependent and ubiquitin-independent proteolytic activity of 26S proteasomes (Murakami *et al*, 1992), did not show decreased proteolytic activity. Rather, the activity was increased 1.4-fold in the hRpn13-knockdown cells (Figure 4C). We also examined ubiquitin-dependent proteolytic activity using *in vitro* ubiquitinated cIAP1 (inhibitor of apoptosis-1), which is a ubiquitin ligase that catalyzes its own ubiquitination for degradation (Yang *et al*, 2000). As shown in Figure 4D, extracts of hRpn13-knockdown cells showed normal proteolytic activity in the degradation of ubiquitinated cIAP1 proteins. IκBα is also a well-known substrate of 26S proteasomes that is rapidly ubiquitinated and degraded in response to TNF-α (Suzuki *et al*, 2000). To check proteasome activities *in vivo*, we monitored the degradation rate of IκBα. hRpn13-knockdown cells showed the same degradation efficiency as control cells (Figure 4E). Considered together, the above results suggest that hRpn13 is not essential for overall protein degradation and viability of mammalian cells.

hRpn13 interacts with UCH37 via its C-terminus

Whereas the N-terminal region of hRpn13 is essential for association with 26S proteasomes (Figure 3), the role of the conserved C-terminal region is still unknown. To elucidate its role, we again used the proteomic approach. Flag-tagged hRpn13ΔN that did not interact with proteasomes (Figure 3) was expressed in HEK293 cells and immunoprecipitated from the cell lysate with anti-Flag antibody, followed by LC–MS/MS analysis. The peptides most abundantly identified were those of UCH37 (also called UCHL5) (Figure 5A), which is reported to be associated with proteasomes in fission yeast, fly, and mammals (Lam *et al*, 1997; Holzl *et al*, 2000; Li *et al*, 2000, 2001; Stone *et al*, 2004). We noticed that both hRpn13 and UCH37 had KEKE motifs at their C-terminal extremities. The conserved C-terminal region of hRpn13 is composed of one typical KEKE at its C-terminus (hereafter referred to as KE2) and one KE-rich region adjacent to KE2, which does not fit the definition of KEKE motif, as proposed previously (Realini *et al*, 1994), but is rich in lysine and glutamic acid residues (hereafter referred to as KE1) (Figure 5B, left panel). A proline residue known as a potent α-helical and β-sheet structure breaker (MacArthur and Thornton, 1991) was located between KE1 and KE2. KEKE motifs are known to mediate protein–protein interactions (Realini *et al*, 1994), and we hypothesized that the interaction between these two molecules was KEKE motif dependent. To test this notion, we expressed Flag-tagged hRpn13, hRpn13ΔKE2 lacking typical KEKE motif, and hRpn13ΔKE1 + 2, which lacked both KE1 and KE2 and thus the entire conserved C-terminal region, in HEK293T cells and immunoprecipitation was achieved with anti-Flag antibody (Figure 5B, right panel). Although the three constructs precipitated nearly the same amount of hα6 and hRpn1, hRpn13ΔKE2 precipitated less amount of UCH37 compared with the wild-type hRpn13, and hRpn13ΔKE1 + 2 did not precipitate UCH37. These results indicate that the conserved C-terminal region is required for the interaction with UHC37.

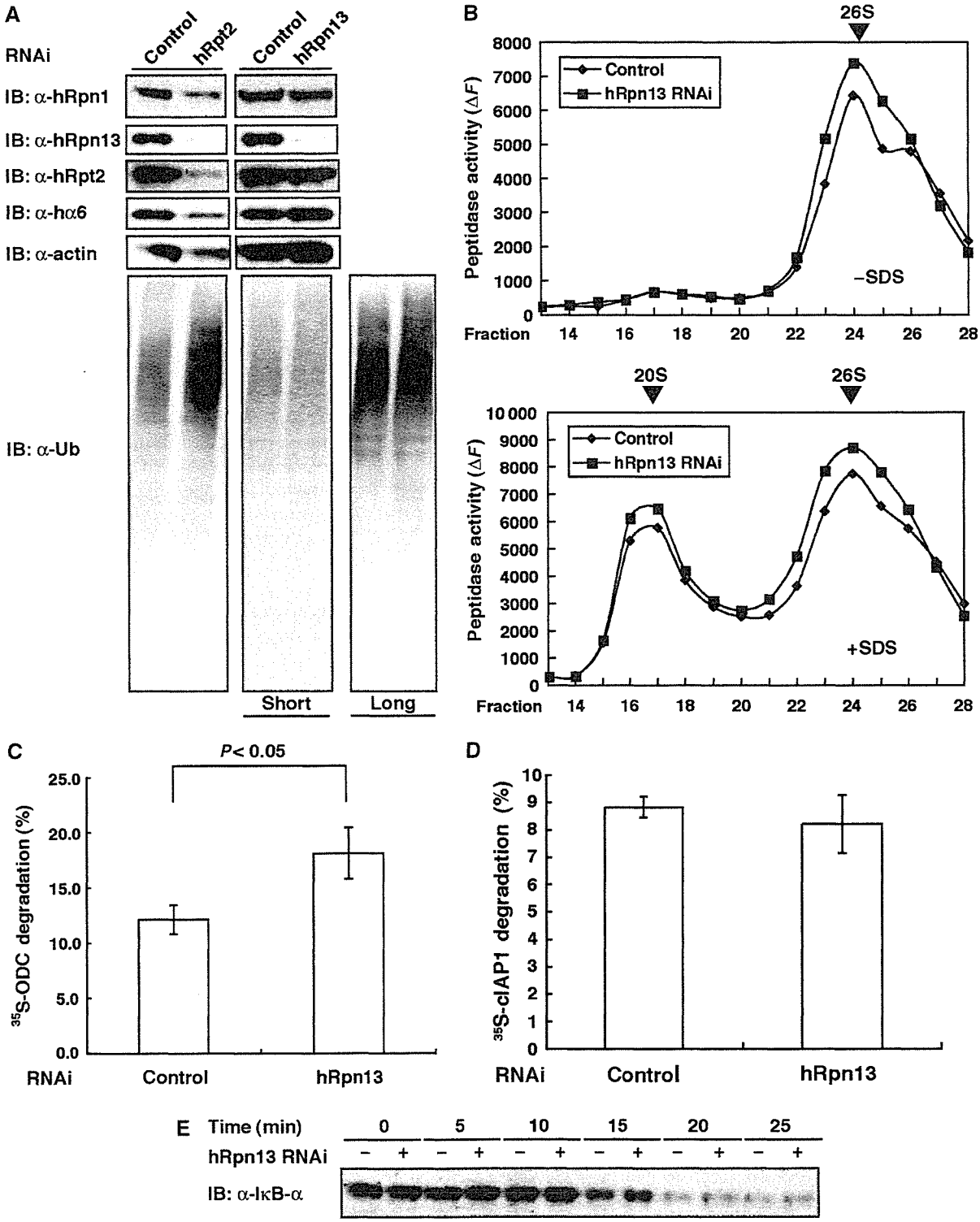

Figure 4 siRNA-mediated knockdown of hRpn13 does not cause proteolytic defects in proteasomes. (**A**) HEK293T cells were transfected with siRNA against hRpn13 or hRpt2. After 48 h for hRpt2 knockdown and 96 h for hRpn13 knockdown, cell extracts were subjected to SDS–PAGE, followed by immunoblotting with the indicated antibodies. (**B**) Extracts of control and Rpn13-knockdown cells were fractionated by 8–32% glycerol gradient centrifugation into 32 fractions from the top. Suc-LLVY-AMC hydrolysis activities were measured in the absence (left) or presence (right) of 0.05% SDS. 20S: 20S proteasome; 26S: 26S proteasome. (**C**) Ubiquitin-independent protein-degrading activity of proteasome. ATP- and AZ-dependent degradation of ^{35}S-labeled ODC protein was assayed. Knockdown cells showed significantly increased activity ($P<0.05$, one-way analysis of variance). Data are mean±s.e.m. values of three independent experiments. (**D**) Ubiquitinated cIAP1-degrading activity of proteasomes. Ubiquitin-dependent degradation of ubiquitinated ^{35}S-labeled cIAP1 was assayed. Data are mean±s.e.m. values of three independent experiments. (**E**) Effect of hRpn13 knockdown on TNF-α-induced degradation of IκBα *in vivo*. HEK293T cells were treated with TNF-α for the indicated times in the presence of cycloheximide. The levels of IκBα proteins were analyzed by immunoblotting.

A

Protein symbol	Protein name	Peptides
UCH37	Ubiquitin carboxy-terminal hydrolase 37	7
TIMM13	Translocase of inner mitochondrial membrane 13 homolog	4
YWHAE	14-3-3 epsilon	4
PRDX1	Peroxiredoxin 1	2
USMG5	Upregulated during skeletal muscle growth 5	2
BUB3	BUB3 budding uninhibited by benzimidazoles 3 homolog	1
TIMM8A	Translocase of inner mitochondrial membrane 8 homolog A	1

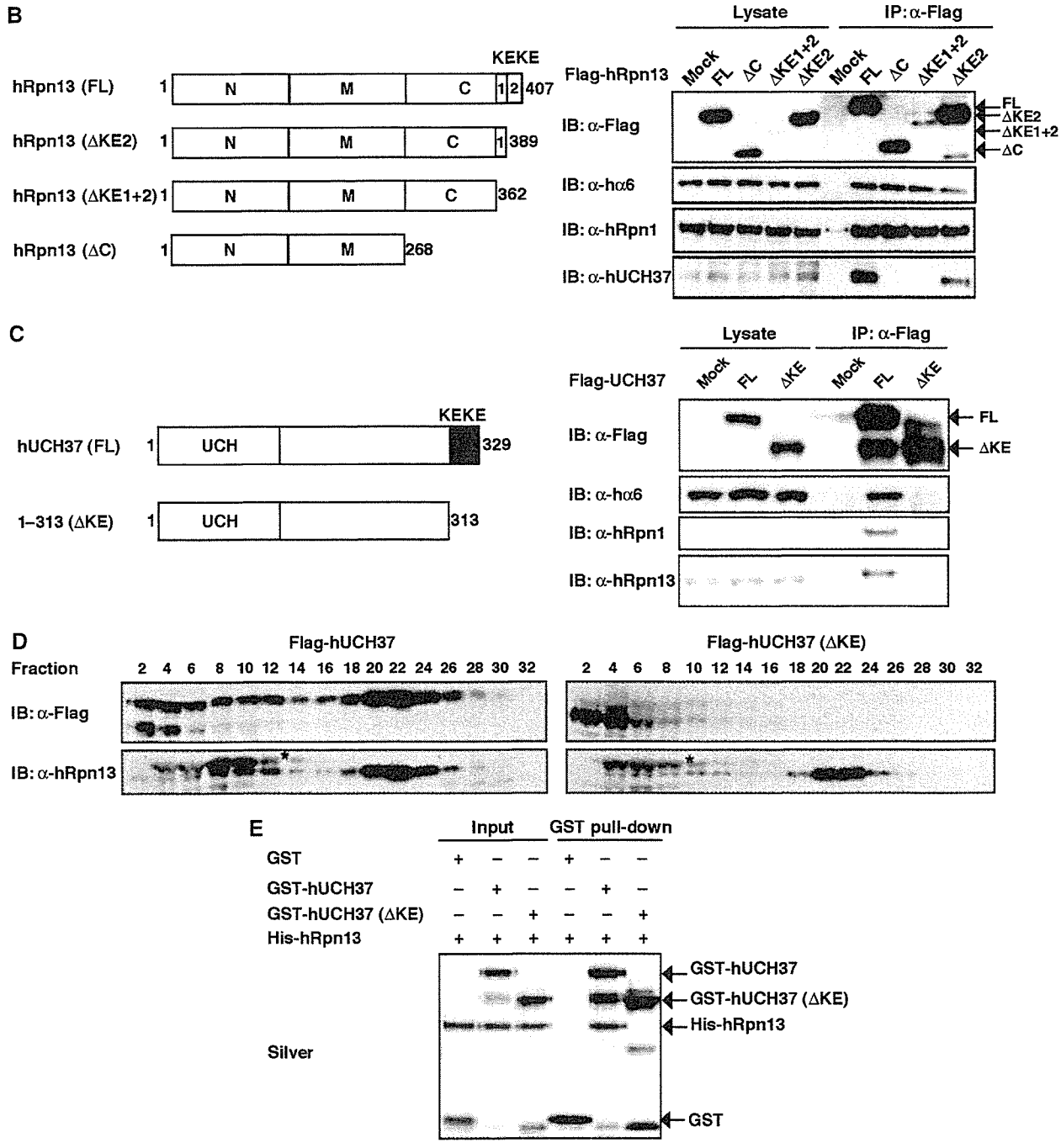

Figure 5 UCH37 interacts with hRpn13. (**A**) A list of proteins detected in four independent hRpn13ΔN immunoprecipitations by LC–MS/MS analysis. The number of identified peptides of each protein is shown. (**B**) Flag-tagged plasmids encoding hRpn13 and its deletion mutants depicted in the left panel were transfected into HEK293T cells. The cell lysates were immunoprecipitated with anti-Flag antibody, followed by immunoblotting for hα6, UCH37, hRpn1, and Flag (right panel). (**C**) Schematic representation of the structures of wild-type UCH37 (FL) and KEKE domain deletion mutant (left panel). HEK293T cells stably expressing Flag-tagged UCH37 (FL), ΔKE, and an empty vector were lysed and subjected to immunoprecipitation with anti-Flag antibody, followed by immunoblot for Flag, hα6, hRpn1, and hRpn13 (right panel). (**D**) The extracts of cells stably expressing Flag-UCH37 and Flag-UCH37ΔKE were fractionated by 10–40% glycerol gradient centrifugation. Immunoblot analysis was performed for each fraction using antibodies against Flag and hRpn13. Asterisks indicate artifact bands. (**E**) GST pull-down analysis of recombinant proteins. GST, GST-UCH37, or GST-ΔKEKE were incubated with 6xHis-Rpn13 and precipitated as in Figure 3C, followed by silver staining.

Next, we examined the role of the KEKE motif of UCH37. As shown in Figure 5C, UCH37 that lacked the KEKE motif (UCH37ΔKE) did not associate with hRpn13 and other proteasome subunits, whereas full-length UCH37 did. Glycerol-density gradient analysis of the extracts showed that a large portion of full-length UCH37 co-sedimented with 26S proteasomes, whereas UCH37ΔKE was observed exclusively in much lighter fractions, presumably as a free form, and that overexpression of UCH37ΔKE did not affect the association of hRpn13 with 26S proteasomes (Figure 5D). In *in vitro* experiments, GST-UCH37 pulled down hRpn13, but GST-UCH37ΔKE did not (Figure 5E), verifying the results depicted in Figure 5C and D. These results indicate that the KEKE motif of UCH37 is necessary for interaction with hRpn13, and hence, with 26S proteasomes.

Knockdown of hRpn13 causes loss of UCH37 proteins

Next, we examined the relationship between hRpn13 and UCH37 in knockdown experiments. We also performed knockdown of USP14, a human ortholog of yeast Ubp6, which is another proteasome-associated DUB (Leggett *et al*, 2002), to examine the relative contributions of UCH37 and USP14 in deubiquitinating activities of 26S proteasomes. Intriguingly, knockdown of hRpn13 caused marked reduction of total cellular UCH37 proteins but not USP14 proteins. On the other hand, knockdown of UCH37 did not affect the level of hRpn13 proteins (Figure 6A). The observed phenotypes of UCH37 knockdown were similar to those of hRpn13 knockdown with regard to cell growth and levels of polyubiquitinated proteins, which were almost the same as the control (Figure 6B and C). Glycerol-density gradient analysis of the extracts of hRpn13-knockdown cells again showed loss of UCH37 proteins in both free and 26S proteasome fractions, with unchanged distributions of proteasome subunits such as hRpn1 and α6 (Figure 6D). Next, we examined the mechanism of decrease in UCH37 proteins in hRpn13-knockdown cells. Control and hRpn13-knockdown cells were treated with various protease inhibitors such as epoxomycin, which is highly specific for proteasomes, MG132, which inhibits both proteasomes and lysosomal enzymes, and E-64d and pepstatin A, which are specific to lysosomal cathepsins. Although these agents worked effectively in inhibiting the relevant proteases (as monitored by the accumulation of polyubiquitinated proteins for proteasome inhibition and accumulation of lipid-conjugated forms of LC3 proteins for inhibition of lysosomal enzymes; Komatsu *et al*, 2005), UCH37 was not increased by any of the inhibitors (Figure 6E). Pulse–chase experiments using HEK293T cells that stably expressed Flag-tagged UCH37 showed almost the same half-life of UCH37 proteins in knockdown cells and control cells (Figure 6F). Semiquantitative reverse transcription–polymerase chain reaction (RT–PCR) showed almost the same expression levels of UCH37 mRNA in hRpn13-knockdown cells and control cells (Figure 6G). Considered together, these results indicate that hRpn13 is required for maintaining normal protein levels of UCH37, and that loss of UCH37 proteins in hRpn13 is not due to metabolic instability of UCH37 proteins or due to repression of transcription of UCH37 mRNA. At present, the mechanism is not clear.

Knockdown of hRpn13 decreases deubiquitinating activities of 26S proteasomes

Finally, we tested the deubiquitinating activities of knockdown cells shown in Figure 6A. As there are abundant DUBs that are not associated with proteasomes, we partially purified complexes of 26S proteasomes and proteasome-associated DUBs by glycerol-density gradient centrifugation, and the 26S proteasome fractions identified by Suc-LLVY-MCA-hydrolyzing activities were used in the following experiments. As shown in Figure 7A, the 26S proteasome fraction of each knockdown cell contained proteasome subunits at a comparable level to each other. Proteins of hRpn13, UCH37, and USP14 were almost completely lost in 26S proteasomes of the cells transfected with siRNAs against hRpn13, UCH37, and USP14, respectively. The deubiquitinating activities of these samples were assayed using ubiquitin-AMC as a substrate. Notably, the deubiquitinating activities of hRpn13- and UCH37-deficient proteasomes were approximately only one-third of those of the control. In contrast, knockdown of USP14 did not significantly reduce the activity. Concomitant knockdown of USP14 with knockdown of hRpn13 or UCH37 did not have additive effects. These results clearly indicate that UCH37 is the dominant DUB associated with mammalian 26S proteasomes and that recruitment of UCH37 by hRpn13 is required for this activity.

Discussion

Adrm1 was originally described as a heavily glycosylated membrane protein of molecular mass 110 kDa (Shimada *et al*, 1991). However, recent studies showed that Adrm1 was hardly, if any, glycosylated and most of it could be detected as a 42 kDa protein (Simins *et al*, 1999; Hasegawa *et al*, 2001; Lamerant and Kieda, 2005). Likewise, the antibody against Adrm1 we raised in this report did not detect the 110 kDa form of Adrm1. Moreover, immunocytochemical analysis of HeLa cells using this antibody indicated that Adrm1 is a soluble protein distributed both in the cytosol and nucleus, which is quite similar to the distribution of proteasomes, as revealed by staining for hRpn1 (Figure 1). Database search analysis suggested that Adrm1 is a human ortholog of yeast Rpn13 subunit. Indeed, Adrm1 was identified in the purified 26S proteasomes at nearly stoichiometric amount, and so we designated it hRpn13. While this manuscript was in preparation, Jorgensen *et al* (2006) reported Adrm1 as a novel proteasome-associated factor (Jorgensen *et al*, 2006). We also identified hRpn2 as an hRpn13-interacting subunit (Figure 3). A previous report mapped the location of p37A (*Drosophila* ortholog of UCH37) in *Drosophila* 26S proteasomes to the interface between the base and the lid, by electron microscopy using gold-labeled ubiquitin-aldehyde bound to the p37A/UCH37 (Holzl *et al*, 2000), which is consistent with our results.

However, immunodepletion analysis showed that not all the 26S proteasomes contain hRpn13 (Figure 2D). In this regard, it is better not to call hRpn13 a subunit of proteasomes but rather regard it as one of the PIPs. Even in yeast, there is no definite evidence to indicate that Rpn13 is a constitutive subunit of proteasomes. In a quantitative mass spectrometric analysis of budding yeast 26S proteasomes, Rpn13 was identified by much smaller number of peptides, compared to authentic proteasome subunits (Guerrero *et al*,

2006). The relatively low homology between Adrm1 and yeast Rpn13 may reflect this fact, as genuine proteasome subunits, but not PIPs, have much higher similarities between human and yeast subunits. Knockdown experiments further revealed that hRpn13 is not essential for proteolysis or viability of mammalian cells, whereas knockdown of hRpt2, a 19S ATPase subunit, was fatal (Figure 4). It is noteworthy that all subunits of RP, except Rpn9, Rpn10,

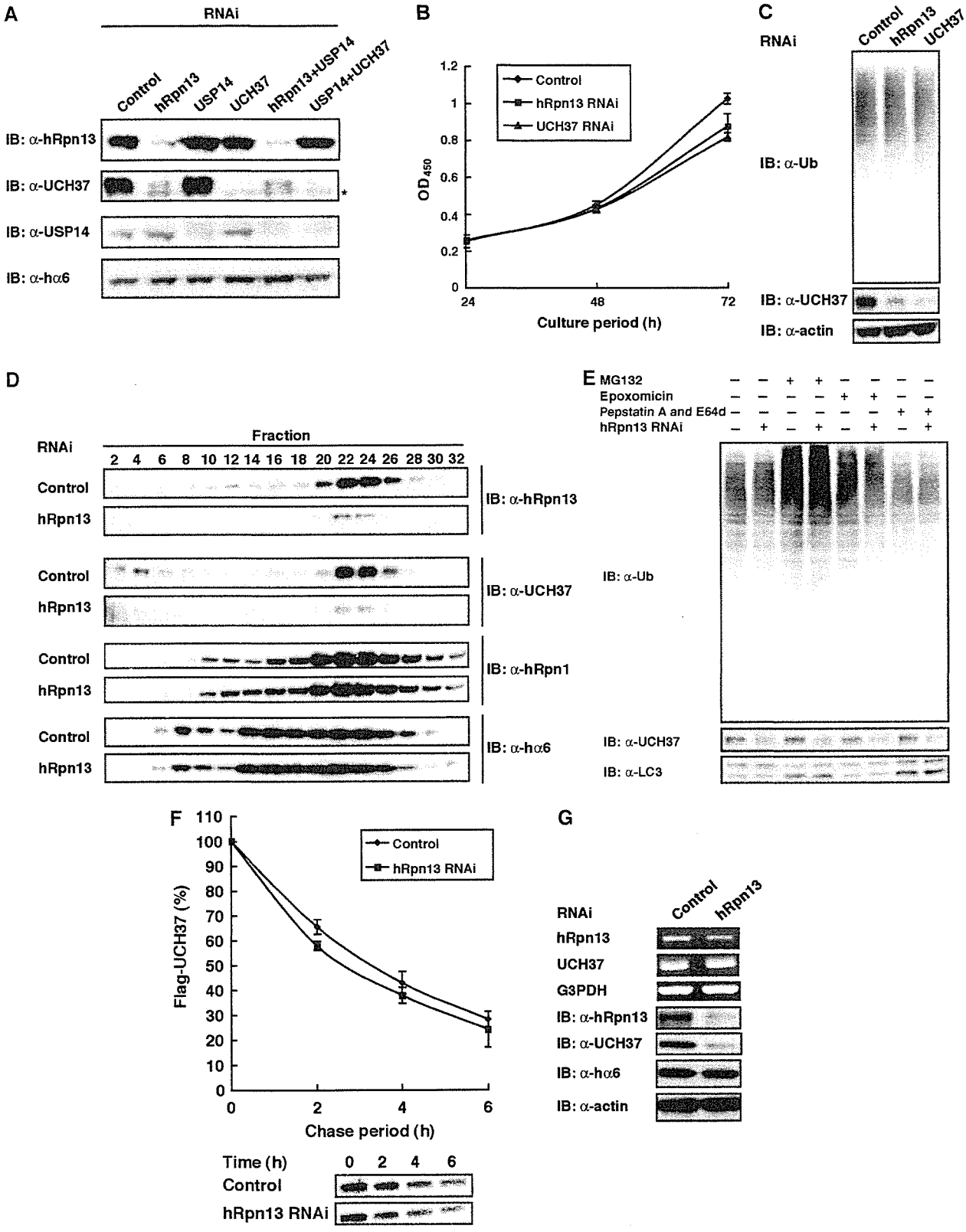

and Rpn15/Sem1, are essential for proliferation of the budding yeast examined so far. Considered together, these results suggest that hRpn13 plays an auxiliary role in the proteasome-dependent protein degradation.

hRpn13 has no known functional motifs and does not seem to be necessary for the structural integrity of proteasomes. Then, what is the role of hRpn13 in proteasomes? hRpn13 can be divided into three functional regions: the N-terminal, C-terminal, and the inserted regions. The former two regions are well conserved from budding yeast to human, whereas the latter one is not found in budding yeast (Figure 1). We proved that the conserved N-terminal region is required for association with proteasomes (Figure 3). We also examined the biological role of the C-terminal region, and our results revealed that it serves as an acceptor for UCH37 (Figure 5). Moreover, loss of hRpn13 proteins caused concurrent loss of UCH37 proteins, indicating that hRpn13 recruits UCH37 to proteasomes and at the same time it is required for maintenance of UCH37 protein levels (Figure 6). As the half-life of UCH37 protein in hRpn13-knockdown cells was similar to that of control cell, the role of hRpn13 in maintaining UHC37 protein levels does not seem to be the stabilization of UCH37 protein. Consistent with this notion, neither the use of a proteasome inhibitor nor a lysosomal inhibitor resulted in accumulation of UCH37 proteins in knockdown cells. The amount of UCH37 mRNA was also unaltered in knockdown cells. At present, we do not know the reason for loss of UCH37 protein in knockdown cells, and the role of the insertion region is yet to be determined. No ortholog of UCH37 is found in budding yeast. Evolutionarily, UCH37 orthologs have emerged synchronously with the insertion region of Rpn13 orthologs. This region may have some role in the relationship with UCH37 and/or other proteins yet to be identified.

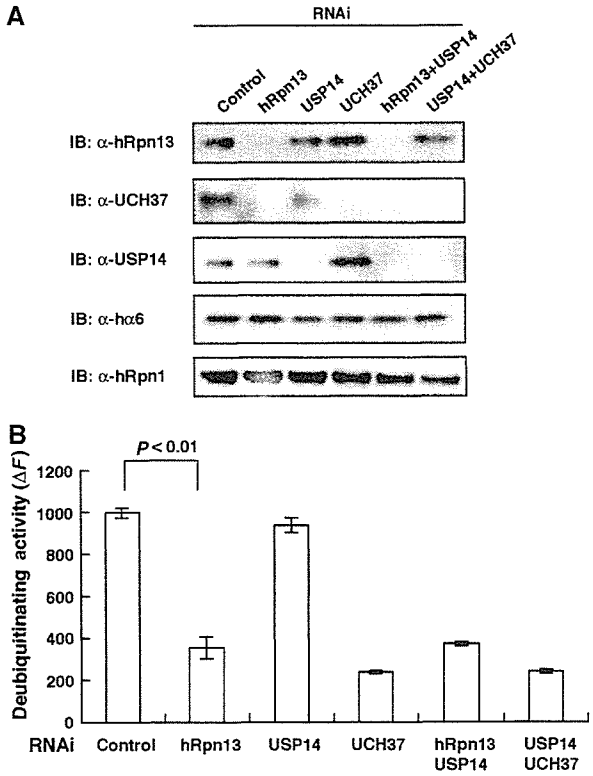

Figure 7 Knockdown of hRpn13 reduces deubiquitinating activities of 26S proteasomes. (**A**) hRpn13 and proteasome associating DUBs in knockdown cells. Cell extracts shown in Figure 6A were fractionated by 10–40% glycerol gradient centrifugation into 32 fractions. Immunoblot analysis of 26S proteasome fractions determined by Suc-LLVY-hydrolyzing activity was performed using the indicated antibodies. (**B**) The deubiquitinating activities of 26S proteasome fractions shown in panel A were measured using ubiquitin-AMC as a substrate. hRpn13- and UCH37-knockdown cells showed significantly reduced deubiquitinating activities ($P<0.01$). Data are mean ± s.e.m. values of three independent experiments.

Ubp6 (USP14 in mammals) is another well-known DUB that associates with proteasomes. A mutation in USP14 in mice causes neurological disorders, demonstrating the importance of USP14 in mammals. Low expression of USP14 in mice is associated with reduced levels of free ubiquitin, suggesting its role in recycling ubiquitins (Anderson *et al*, 2005), as is also suggested in studies in budding yeast (Guterman and Glickman, 2004). However, the deubiquitinating activity of proteasomes is mainly attributed to UCH37 in fission yeast (Stone *et al*, 2004). Our present study also demonstrates that the deubiquitinating activities of 26S proteasomes are affected more profoundly by loss of UCH37 than USP14, indicating that UCH37 is the dominant DUB over USP14 in mammalian proteasomes. Recruitment of UCH37 by hRpn13 is essential for the activity of UCH37, as hRpn13 knockdown resulted in loss of UCH37, followed by a decrease in the deubiquitinating activity of 26S proteasomes at a level comparable to UCH37 knockdown. Further studies are required to distinguish the roles of USP14 (Ubp6) and UCH37 in organisms that have both molecules. It is plausible that the two molecules have distinct roles.

Despite the significant reduction of deubiquitinating activity of hRpn13-deficient proteasomes, they efficiently

Figure 6 Knockdown of hRpn13 causes loss of UCH37 proteins. (**A**) HEK293T cells were transfected with siRNA against hRpn13, UCH37, or USP14. Where indicated, cells were transfected with a mixture of siRNAs. After 96 h, cell extracts were subjected to SDS–PAGE, followed by immunoblotting with the indicated antibodies. (**B**) Growth rates of hRpn13 knockdown, UCH37 knockdown, and mock cells. The cells were seeded in triplicate in 96-well dishes on day 0 (72 h after transfection), cultured in normal growing medium, and their proliferation was measured every 24 h. Data are mean ± s.d. values. (**C**) Cell extracts of hRpn13 knockdown, UCH37 knockdown, and mock cells were subjected to SDS–PAGE, followed by immunoblotting with the indicated antibodies. (**D**) Samples fractionated by 10–40% glycerol gradient centrifugation were immunoblotted with the indicated antibodies. (**E**) Lack of accumulation of UCH37 proteins in hRpn13-knockdown cells following inhibition of the proteasome or lysosomal cathepsins. HEK293T cells transfected with siRNA were treated with MG132 (50 μM, 2 h), epoxomycin (1 μM, 12 h), or E-64 and pepstatin A (10 μg/ml, 12 h). The cells were lysed and subjected to immunoblot. (**F**) Pulse–chase analysis of Flag-UCH37. HEK293T cells stably expressing Flag-UCH37 were pulse-labeled for 30 min with ^{35}S-labeled methionine and chased for the indicated time periods. After immunoprecipitation with M2 agarose, samples were separated by SDS–PAGE and autoradiographed (bottom panels). The upper panel shows the results of band quantitative analysis. Data are mean ± s.d. values of three independent experiments. (**G**) hRpn13 knockdown does not alter UCH37 mRNA transcription. Semiquantitative RT–PCR (the upper three panels) and immunoblotting (the lower three panels) were performed using total RNA and proteins extracted from control and hRpn13-knockdown cells 48 h after transfection with siRNAs.

degraded substrate proteins such as ODC, ubiquitinated c-IAP, and IκBα (Figure 4). These observations seem to be in marked contrast to the case of yeast Rpn13, whose deletion caused a complete defect in degradation of a UFD substrate (Verma *et al*, 2000). However, as yeasts that lack Rpn13 are viable (Winzeler *et al*, 1999), the proteolytic defect is probably specific to UFD substrates. Rpn13 may recruit a component essential for degradation of UFD substrates in yeast. The precise role of hRpn13 and UCH37 still remains elusive. Curiously, knockdown of hRpn13 significantly increased the degrading activity of ODC but not that of ubiquitinated cIAP1 protein *in vitro* and IκBα *in vivo*. As sole knockdown of UCH37 did not increase the degrading activity of ODC (data not shown), the results observed in hRpn13 knockdown are not simply due to loss of UCH37. hRpn13 may influence access of protein to the channel of ATPase rings of proteasomes by sitting in the space between the base and lid (Holzl *et al*, 2000), or may recruit proteins that are relevant to proteolysis other than UCH37. At least from these results, both hRpn13 and UCH37 do not seem to be generally required for protein degradation by 26S proteasomes. It is assumed that UCH37 disassembles polyubiquitin chains from the distal end, shortening it such that the attached proteins can be released from the proteasome if there is a delay in efficient degradation (Stone *et al*, 2004). hRpn13 and UCH37 may be important in some specific situations. Further studies are required to determine the specific functions of hRpn13 and UCH37.

Materials and methods

Plasmids and cloning

The complementary DNAs (cDNAs) used in the present study were obtained by RT–PCR from total RNA isolated from HeLa cells or mouse livers using Superscript III (Invitrogen, San Diego, CA) and Pyrobest DNA polymerase (Takara Shuzo, Ohtsu, Japan). All amplified fragments were cloned into pcDNA3.1 vector (Invitrogen) and sequenced for confirmation. Deletion mutants (hRpn13ΔC, ΔN, N, ΔKE1 and ΔKE1 + 2, and UCH37ΔKE) were generated by PCR from wild-type hRpn13 and UCH37 and the Flag tag was introduced at the N-terminus of the constructs. For expression of GST and 6xHis fusion proteins, the cDNAs were subcloned into pGEX6P-1 (Amersham Life Science, Buckinghamshire, UK) and pET-28a (Novagen, Madison, WI) vector, respectively.

Immunological analysis

For immunoprecipitation analysis, HEK293T cells were transfected with plasmids using Fugene 6 (Roche, Mannheim, Germany). After 36 h, the cells were lysed with ice-cold phosphate-buffered saline (PBS) containing 1% Nonidet P-40 (NP-40) and centrifuged at 20 000 *g* for 10 min at 4°C. The supernatant was added with M2-agarose (Sigma Chemical Co., St Louis, MO) and rotated for 1 h at 4°C. The immunoprecipitates were washed five times with ice-cold PBS containing 0.5% NP-40 and then boiled in SDS sample buffer in the presence of β-mercaptoethanol (β-ME). Samples were subjected to SDS–PAGE, transferred to polyvinylidene fluoride membrane, and analyzed by immunoblotting with anti-Flag (M2; Sigma). Polyclonal antibodies against hRpn1, hRpn10, hRpt2, hRpn13, UCH37, and USP14 were raised in rabbits using recombinant proteins expressed in and purified from BL21RIL strain (Novagen) as GST fusion proteins: mouse Rpn1 (full length), mouse Rpn10 (residues 1–251), hRpt2 (residues 1–82), hRpn13 (residues 361–407), mouse UCH37 (residues 228–329), and human USP14 (full length). Anti-LC3 antibody was described previously (Komatsu *et al*, 2005). The antibodies for polyubiquitin and actin were purchased (FK2; MBL, Ina, Japan, Chemicon International Inc., Temecula, CA). All experimental protocols described in this study were approved by the Ethics Review Committee for Animal Experimentation of Tokyo Metropolitan Institute of Medical Science.

GST pull-down assay

Recombinant GST- or 6xHis-tagged proteins were produced in *Escherichia coli* and purified with glutathione Sepharose 4B (Amersham) or Ni-NTA Sepharose (Qiagen, Hilden, Germany). After elution of proteins from the beads, the preparations were dialyzed against buffer A (50 mM Tris–HCl (pH 7.5), 150 mM NaCl, 5 mM β-ME, and 10% glycerol). In GST pull-down analysis, 5 μg of each sample was mixed in 600 μl of buffer A and constantly rotated for 1 h at 4°C, and then 30 μl of glutathione Sepharose 4B was added and further rotated for 1 h. After washing with buffer A, bound proteins were eluted with 10 mM glutathione and subjected to SDS–PAGE, followed by immunoblot and silver staining (Wako Pure Chemical Industries, Osaka, Japan).

RNAi experiments

siRNAs targeting hRpt2, hRpn13, UCH37, and USP14 with the following 25-nucleotide sequences were purchased from Invitrogen: Rpt2, 5′-GGAGUACGAUGUGUAAGUGCCCAUU-3′; Rpn13, 5′-GGA GGGUCUACGUGCUGAAGUUCAAA-3′; UCH37, 5′-ACCGAGCTCAT TAAAGGATTCGGTT-3′; USP14, 5′-UCAGCAUCGUAACACCAGAA GAUAU-3′. siRNAs were transfected into HEK293T cells with Lipofectamine 2000 (Invitrogen) at a final concentration of 2 nM in six-well dishes. The cells were analyzed 96 h (hRpn13, UCH37, USP14, hRpn13 + USP14, and USP14 + UCH37) or 48 h (hRpt2) after transfection. For protease inhibition assay, HEK293T cells transfected with siRNA (96 h) were cultured in the presence or absence of protease inhibitors (50 μM MG132 for 2 h, 10 μg/ml E64d and 10 μg/ml pepstatin A for 12 h, or 1 μM epoxomycin for 12 h). Cell growth was measured using Cell Counting Kit-8 (Wako) according to the instructions provided by the manufacturer. Briefly, cells were seeded at 1×10^3 cells/well in 96-well plates. Absorbance was measured using Microplate reader (Bio-Rad).

Glycerol-density gradient analysis

Mouse livers were homogenized in a Potter-Elvehjem Homogenizer in buffer B (in mM, 25 Tris–HCl (pH 7.5), 2 ATP, 5 $MgCl_2$, and 1 dithiothreitol). HEK293T cells were lysed in buffer B containing 0.2% NP-40. The homogenates and lysates were clarified by centrifugation at 20 000 *g* and subjected to 10–40% (v/v) or 8–32% (v/v) linear glycerol-density density gradient centrifugation (22 h, 83 000 *g*) as described previously (Hirano *et al*, 2005).

In vitro assay of proteasome activity

Proteasome peptidase activity was measured using a peptide substrate, succinyl-Leu-Leu-Val-Tyr-7-amino-4-methyl-coumarin (Suc-LLVY-MCA), and the degradation of the recombinant ^{35}S-labeled ODC was assayed in the presence of ATP, an ATP-regenerating system, and AZ, as described previously (Hirano *et al*, 2005). For the assay of cIAP1 degradation, cDNAs encoding Flag-cIAP1 subcloned into pcDNA3.1 were transcribed *in vitro*, translated, and radiolabeled as described previously (Hirano *et al*, 2005). The ^{35}S-labeled Flag-cIAP1 was purified using M2-agarose (Sigma) and eluted with Flag-peptide (Sigma). For ubiquitination of cIAP1, 3 000 000 c.p.m. of ^{35}S-labeled cIAP1, 0.25 μg of E1, 0.9 μg of UbcH5, and 33 μg of ubiquitin (Sigma) were mixed and incubated in a volume of 80 μl for 90 min at 30°C, as described previously (Murata *et al*, 2001). Finally, 2.5 μl of the ubiquitination mixture was added to 10 μl of cell lysates in the presence of 2 mM ATP, incubated at 37°C for 20 min, and then radioactivities of trichloroacetic acid-soluble fractions were measured.

TNF-α-dependent IκBα degradation

HEK293T cells transfected with siRNA were treated with 100 μg/ml cycloheximide (Sigma) for 10 min, and then human TNF-α (Genzyme, Cambridge, MA) was added at a final concentration of 10 ng/ml. Changes in the protein levels of endogenous IκBα after treatment with TNF-α were analyzed by immunoblotting with anti-IκBα (c-21) (Santa Cruz Biotechnology, Santa Cruz, CA).

Deubiquitination assay

For ubiquitin-7-amino-4-methylcoumarin (ubiquitin-AMC) (Boston Biochem) hydrolysis assays, 10 μl of 26S proteasome fraction separated by glycerol gradient centrifugation was incubated with 0.25 μM ubiquitin-AMC for 15 min at 37°C. The release of AMC was measured fluorometrically.